Single-Molecule Experiments on Biological Nanopores Embedded on a Capillary

Masters thesis, Nanobiotechnology

Dainora Jankūnaitė

June 10, 2019

AALBORG UNIVERSITY
STUDENT REPORT

Final thesis for masters studies of Nanobiotechnology at the School of Engineering and Science

The Faculty of Natural Sciences

Physics and Nanotechnology
Skjernvej 4a
9220 Aalborg Ø

Title:
Single-molecule experiments on biological nanopores embedded on a capillary

Project period:

February 2019 - June 2019

Participant:

Dainora Jankūnaitė

Supervisors:

Leonid Gurevich (Aalborg University)

Sanjin Marion (École polytechnique fédérale de Lausanne)

Jens Gundlach (University of Washington)

Host professor:

Aleksandra Radenovic (EPFL)

Host laboratory:

Laboratory of Nanoscale Biology (EPFL)

Total pages: 49
Finalized 10-06-2019

Abstract:

Enzymatic nucleic acids translocation are essential for biological functions, such as chromosome maintenance, DNA replication, transcription and repair. There have been many methods developed for kinetic studies of nucleic acids motor proteins. Recently emerged an unforeseen resolution single-molecule technique called single-molecule picometer resolution nanopore tweezers (SPRNT). The technique can resolve minuscule temporal steps. ForceS magnitude acting on a nucleic acid affect proteins kinetics. This force is not known in SPRNT setup.
The objective of this thesis was to measure the force using optical tweezers (OT). To design the experiment we had to devise the flow cell, design the DNA construct and optimize the lipid bilayer formation.
In the study, we used optical tweezers and capillary combination. We formed lipid bilayers at the capillary opening and reconstituted MspA pore there. We compared the current-voltage characteristics of the pore in our flow cell and in SPRNT setup. We also demonstrated that the OT is compatible with the biopore and lipid bilayers in our flow cell.

Contents

1 Introduction

Many of the most important biological functions of cells are dependant on enzymes' ability to translocate nucleic acids. Motor proteins, such as helicases [1], polymerases [2], chromatin remodelers [3], restriction enzymes[4] and nucleases[5] are responsible for processes like chromosome maintenance, DNA replication, transcription and repair[6, 7]. The enzymes use the chemical potential energy obtained from interactions with nucleoside triphosphates to perform mechanical work - directional nucleic acids translocation. In order to understand the translocation mechanisms quantitative kinetic information is needed[8].

Study methods of biomolecular interactions can be categorized based on whether the molecules were tested individually or in bulk. The two types are an ensemble and single-molecule techniques. Ensemble studies are inherently high-throughput designed to study millions of molecules simultaneously. Although they provide statistically significant results, some processes can only be observed by studying a single molecule at a time.

Single-molecule techniques are designed to study biomolecular processes with high-resolution. Also, it can be used for mechanical manipulation, such as stretching and applying torsion on a molecular level[9]. Optical tweezers are one of the most popular single-molecule techniques, which can apply and measure the force acting on a biomolecule. Protein structure[10] and activity[11] depends on its environment, and any forces acting on it from its surroundings. Therefore, it is a very important characteristic to know in enzymes, such as motor proteins.

While optical tweezers are very versatile and can be used to study motor protein kinetics, it is not the most precise tool for this application. Recently a single-molecule technique based on nanopore sequencing was developed. It is called single-molecule picometer resolution nanopore tweezers (SPRNT). In SPRNT, negatively charged DNA is moving towards a positive electrode on the other side of the pore. The DNA is translocated in a controlled manner by a step-wise moving motor protein. Here, the DNA sequence is known. By measuring the current levels and knowing the distance between the protein and the pore constriction, one can deduce the exact location of the motor protein on the DNA. The method offers unforeseen spatiotemporal resolution, but the net force acting on DNA in this system is not known, which is an important condition affecting a motor protein behaviour in SPRNT.

To address the issue, we are developing a method to measure the equivalent of the net force acting on DNA in SPRNT using optical tweezers. The long term goal is to calibrate the force to voltage, temperature, salt concentration and other parameters. The calibration allows us to infer from the current the forces in the measurement. To understand the force experiment development, single-molecule techniques, nanopores, nanopore sequencing, SPRNT and lipid bilayer formation techniques will be introduced.

1.1 Single-molecule techniques

In our study, we combined two methods for individual molecule studies, known as single-molecule techniques: optical tweezers (OT) and single-molecule picometer resolution nanopore tweezers (SPRNT). SPRNT is a tool, suited to measure nucleic acid motor protein dynamics. While optical tweezers have a broad range of applications, we chose it for determining the force exerted on DNA in a SPRNT measurement. In this section, we will discuss these and a few other single-molecule techniques.

Single-molecule technique development plays a big role in the understanding of biochemical dynamics. For a while ensemble techniques used to be the only way to study biomolecular processes. In ensemble techniques, molecular changes are averaged over a great number of molecules (up to a few moles). The averaging is a double-edged sword - it provides statistically significant results, but small or transient steps are inevitably masked. Single-molecule experiments are good to study specifics of systems unavailable when an ensemble of millions of particles is studied. In cases, where the sample population has a few normal distributions (called multimodal distribution), averaging over the whole population would give meaningless results. For instance, measuring an ensemble of enzymes having an on-off states, e. g. ion current of channel proteins in open and closed states would result is average current value, which cannot be attributed to any state. Single-molecule techniques are particularly useful for complex processes involving multiple steps and enzyme activity deviating from a standard Michaelis-Menten behaviour[12]. The ability to study individual molecules in real-time has opened an avenue for more accurate measurements of biophysical quantities, including conformational changes[13, 14], polymer's dynamic properties[15], as well as physicochemical interactions with other molecules and surfaces[16–18].

To date, there have been a number of methods developed to study single molecules. In the 1970s the technique called patch clamp sensing was designed to study ion channels in biological membranes[19]. Soon, other, more versatile techniques were developed allowing nanomanipulation and force measurements. The three most common techniques are namely atomic force microscopy (AFM), magnetic tweezers (MT) and optical tweezers (OT).

The AFM is a type of scanning probe microscope usually used to study surface characteristics. In AFM, a cantilever is normally used to scan the probe attached to a substrate line by line, where the forces applied to the sample due to their interaction with the probe are measured by cantilever deflection. For polymeric molecule pulling experiments, the molecule attached to the substrate surface is pulled by one end bound to a cantilever. A stage moves away from the cantilever and the molecule is stretched (Figure 1.1 a). The AFM cantilever tends to unspecifically bind the probe. The tip can unwantedly bind to different molecules or non-specific positions, making it complicated to analyze the results in pulling experiments. Therefore, for nucleic-acid pulling, the polymer ends and

the cantilever is modified with ligand-receptor (e.g. biotin-avidin) or antibody-antigen pairs. There have been significant enhancements made to meet specific requirements of different experiments and AFM has been widely used over several decades[20].

Magnetic tweezers is a very direct force spectroscopy technique. It has two main components: magnet and a camera. The magnet is used to manipulate a sample bound to a magnetic bead, while the camera tracks the real-time position of the bead. A magnetic particle is attached to the molecule of interest and manipulated using a magnetic field, which makes it a highly selective technique[20] (Figure 1.1 b). Also, it allows to readily make measurements on multiple single molecules in parallel. The simple configuration and sample specificity make it a very popular tool in biophysics.

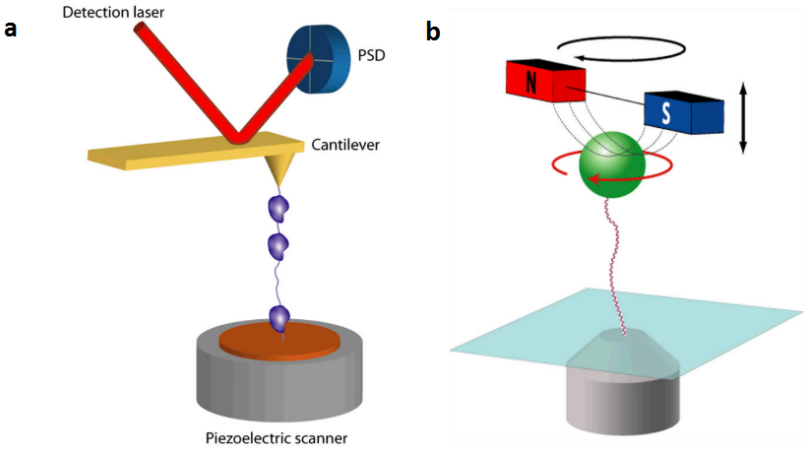

Figure 1.1: Force spectroscopy techniques in use for biological single molecule experiments. (a) Schematic of an AFM. A protein molecule is attached to the substrate and the AFM cantilever tip. The force exerted on the molecule is measured by the cantilever deflection, which is obtained from the displacement of the low power laser reflection on a position sensitive device (PSD). The piezo stage moves in z direction, continuously increase the distance between the substrate surface and the cantilever. The distance between the AFM tip and the sample surface gives the extension of the molecule. (b) Schematic of a general magnetic tweezers setup. To manipulate DNA using a magnetic field induced by a pair of paramagnets, the molecule is attached to a superparamagnetic bead. A microscope objective is used for tracking the position of the bead. The figures were reproduced from [20].

1.2 Optical tweezers

Optical tweezers (OT) were first demonstrated by Askhin et al in 1986[21]. It is an optical trap based on a single laser beam. Such intense monochromatic light can hold dielectric nano- and macro- particles in one particular point in space like tweezers. Later it became one of the most popular label-free techniques for single molecule studies in biology capable of trapping different biological objects from cells[22] to macromolecules[23]. This flexibility allows using OT to study nucleic acids[9], proteins[24] and DNA-protein interactions[25]. For these reasons, OT was chosen as a measurement tool in our study.

A laser beam is able to trap dielectric particles due to the forces arising from intense light momentum, namely scattering and gradient forces[21]. Scattering force moves the particle in the same direction as the photon flux direction, while the gradient force stabilizes the particle in the middle of the beam. The particle made of a material which refraction index is higher than that of the surrounding medium is pushed by the scattering force in the direction of propagation of the light (Figure 1.2 b). While some photons are reflected by the particle, others interact with it and transfer some of their momenta to the particle. The gradient force of a laser beam with a Gaussian intensity profile traps the particle in the centre of the beam. When the particle is displaced to the edge of the beam, the bigger part of the light is refracted to the same side where the bead is than to the other directions. Therefore, there is a net momentum of light with the direction to that side. Due to the conservation of momentum, the bead is pushed to the opposite direction. Constant pushback from the sides keeps the particle in the middle of the beam (Figure 1.2 a). A microscope objective is used to focus the beam in the focal plane, increasing the gradient force. When the particle is located between the light source and the focus, the scattering force pushes it to the focus. There the gradient force is greater than the scattering, thus the particle cannot propagate farther and is trapped in all three spatial dimensions.

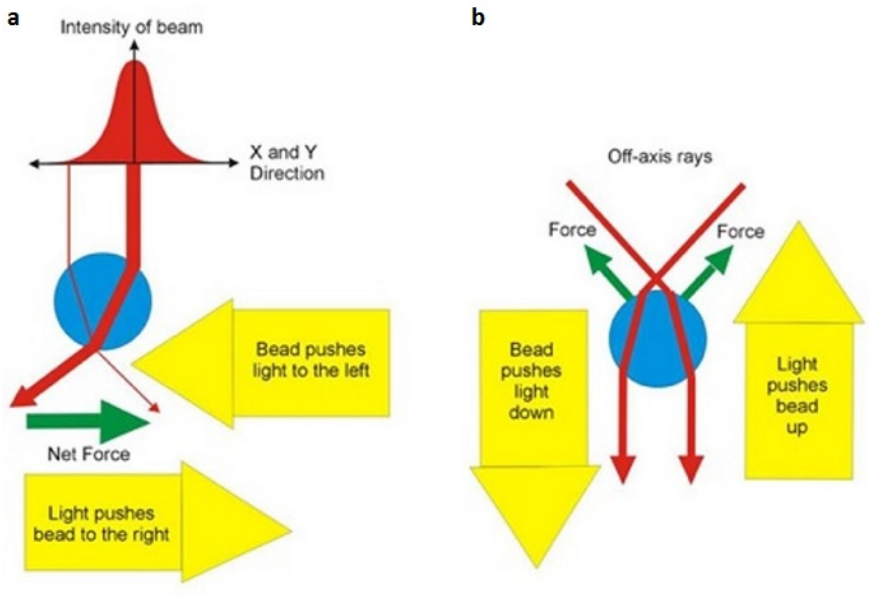

Figure 1.2: A diagram showing gradient (a) and scattering (b) forces acting on a dielectric particle trapped by a laser beam. The gradient force pushes the particle to the most intense part of the beam. The scattering force pushes the particle in the direction of propagation of the light. The gradient force in the trap must be bigger than the scattering force to stabilize the particle in space. The figure was adapted from [**insights.globalspec.com**].

There are two main optical trapping regimes depending on whether the trapped object is larger (ray optics regime) or smaller (Rayleigh regime) than the wavelength of the light. In the ray optics regime, the gradient force always restores the bead towards the focus, whether the particle was displaced above, below or to the side of it (Figure 1.3 a,b,c). When the radiation interacts with an object much smaller than the laser wavelength, the particle acts like an induced dipole, minimizing its energy in the focus of the beam (Figure 1.3 d).

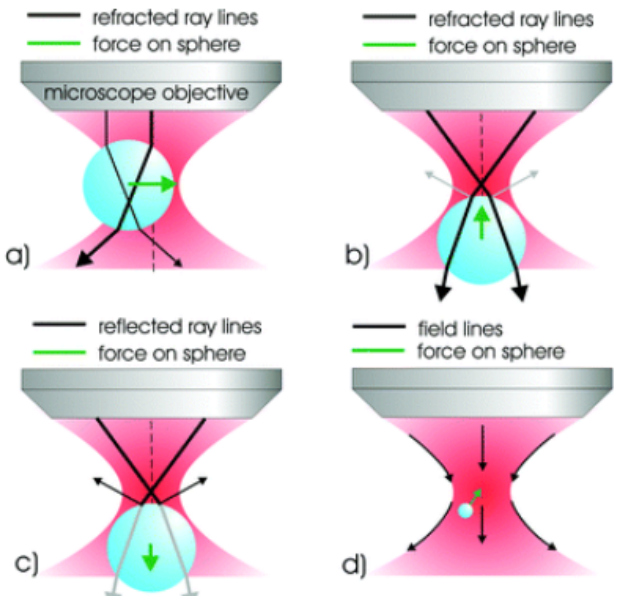

Figure 1.3: Diagram of the optical trapping principles in ray optics and Rayleigh regimes. Ray optics regime: In the case of perpendicular (a) or lateral (b), displacement, the light is refracted from the particle and momentum is partially transferred to the particle. The momentum is conserved, pushing the particle to the middle of the beam until it reaches equilibrium. In the lateral displacement, radiation pressure on the capillary surface can destabilize the trap (c). (d) In the Rayleigh regime, the particle is polarized. A dipole is induced in the particle by the electric field of the light. The dipole is aligned to the high field gradient region in the focus of the beam. The figure is reproduced from [26].

One of the greatest features of optical tweezers is the ability to apply and measure forces acting in the range from a few fN to ∼100 pN, which is sufficient for the unfolding of molecules, e.g. by stretching. Force is one of the fundamental parameters in the biochemical processes inside cells. Mechanical forces have direct influence on the development and differentiation of cells[12]. Forces regulate enzymes' activity[11], protein structure and kinetics[10, 27], changes molecular bonds[28] and other biochemical parameters.

In OT experiments, the forces exerted on the trapped object cannot be measured in a straightforward way. Close to the light focus, the optical trap has properties similar to a linear spring - the force on the particle is proportional to its displacement from the centre of the trap. In experiments, the displacement is measured using a camera or a photodiode. Another important factor is the stiffness of the optical trap known from the OT calibration. The calibration can be done by measuring the thermal fluctuations power spectral density of the particle[29] or the fluid movements induced drag force acting on the particle[30]. The force can then be calculated using a simple formula $F=-k\Delta x$. Here k is the stiffness of the optical trap known from the OT calibration, and Δx is the bead displacement.

Optical tweezers have a number of configurations which are used for different types of assays[31]. Double trap or a single trap combined with a micropipette are commonly used for nucleic acids and motor protein interactions[10, 32]. Protein's interaction with DNA control genetic information storage and accessibility by regulating processes such as chromosome folding, DNA replication, transcription and repair[6]. In the double trap experiments, one optical bead is trapped by a high stiffness OT trap, while the protein on the DNA is attached to a bead in a low-stiffness trap. As the protein moves along the DNA, the distance between the beads decreases and the bead is displaced from a low-stiffness trap centre (Figure 1.4).

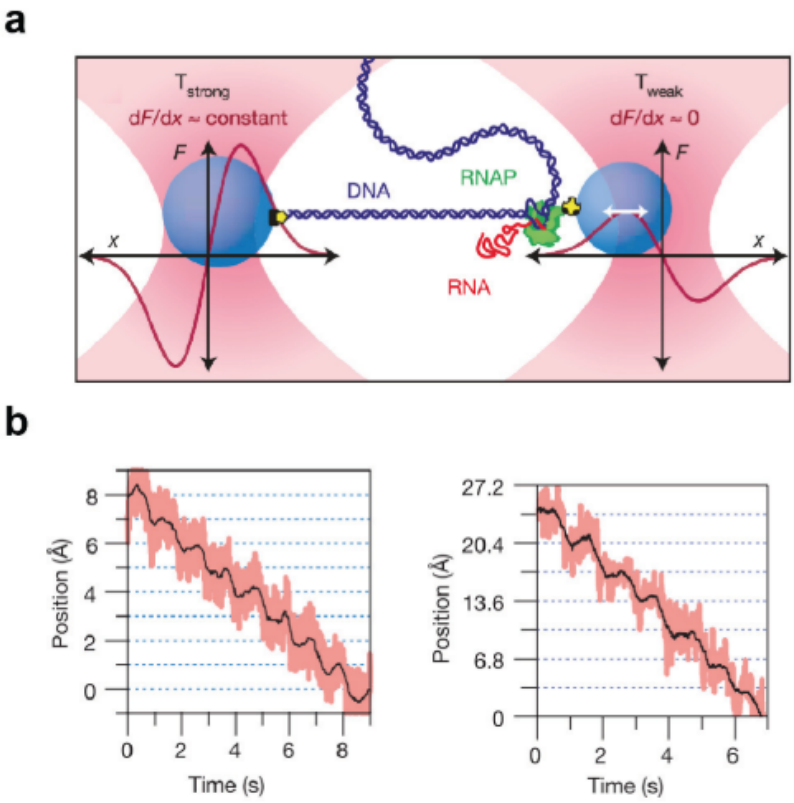

Figure 1.4: RNA polymerase (RNAP) kinetic measurement. (a) Double trap schematic setup. The protein walking on DNA is attached to a weakly trapped bead. The other DNA end is attached to a strongly trapped bead. (b) RNAP position on the DNA in respect with the time. The figure is reproduced from [33].

The most sensitive dual-trap OT configuration designed to measure motor protein dynamics can resolve ∼300 pm steps with the time scale of ∼1 ms[33]. Although, there the noise prohibits an accurate localization. One of the noise sources is Brownian motion of the trapped bead induced by thermal forces, which are always present in experiments conducted in liquids. Another cause of inaccuracy is the instrumental noise, which arises from electronic noise in the photodiode, mechanical vibrations, thermal drifts and laser instabilities. The temporal resolution in OT is limited by instrumental temporal response

and mostly by relaxation time. Relaxation happens when the system is agitated from its equilibrium, i.e. protein conformational changes due to trap displacement, and the particle rapidly moves to a new equilibrium state. This process has a time constant which is the limiting factor in temporal resolution, as the movements shorter than the relaxation time cannot be observed. The relaxation time depends on the rigidity of the molecules, but it is usually determined by the stifness of the trap[31].

The other OT technique for motor protein studies employs nanocapillaries. This method cannot be explained without firstly introducing nanopores and their properties.

1.3 Nanopores

A nanopore is a nanoscale opening in a membrane spanning two reservoirs containing electrolyte solution. In nanopore experiments, the two chambers are connected to different electrodes and a voltage is applied, driving the ions and charged particles through the pore, resulting in a stable current flow[34] (Figure 1.5 a). Nanopores can be used in numerous ways, e. g. as powergenerators[35], water desalination components[36], and nanoreactors[37]. Upon application of an electric field, charged polymeric molecules, such as DNA[38], RNA[39] and polypeptides[40] can be translocated through nanopores. This property allows using them in sensing as a high throughput single-molecule technique. Furthermore, such pores naturally occur in biological cells and can be easily mimicked using nanopores in synthentic pore materials.

Nanopore-based sensing relies on the fact that molecules have a defined volume, therefore when compounds translocate through the pore, they partially block it. Consequently, fewer charges can move through the nanopore and the current drops with the difference associated with the size of the blocking object (Figure 1.5 b). Depending on the length of the object, a characteristic dwell time can be observed. For copolymers, monomers and their order can be resolved from the current drops. Each monomer excludes a particular area in the pore, then a different number of ions can pass through the pore, consequently changing the distinct resistance of the pore (Firgure 1.5). This experiment is particularly useful for nucleic acids sequencing, where one can monitor the signal from a translocating particle and from that infer the sequence of the genome[41].

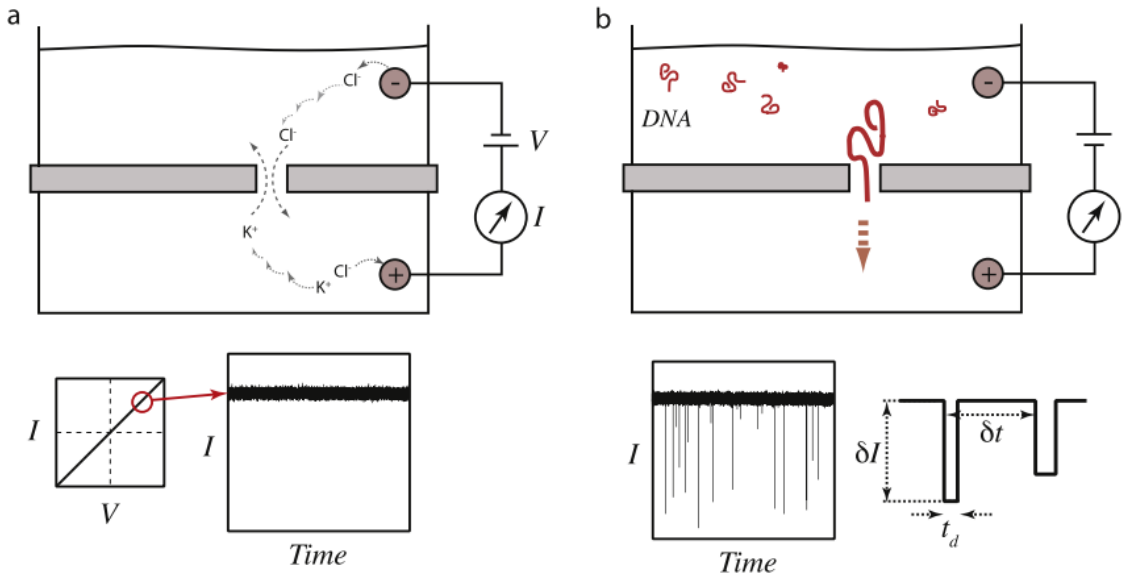

Figure 1.5: Schematic of nanopore sensing. (a) Upon voltage application across a pore, ions start moving through the pore, producing an electrical current. A symmetric pore typically has linear current-voltage behaviour, and at constant voltage the current signal is steady. (b) Charged polymers (here DNA) translocate through the nanopore partially blocking it and increasing resistance. Dwell time (t_d), the average event amplitude (δI) and the time span between successful events (δt) are the main parameters helping the identification of the molecule. The figure is reproduced from [34].

Based on their origin nanopores are categorized into solid-state and biological. Solid-state pores are usually fabricated using clean-room technologies in structures made of silicon nitride (Si_3N_4)[42], silicon dioxide (SiO_2)[43], aluminum oxide (Al_2O_3)[44], boron nitride (BN)[45], graphene[46], polymer membranes[47], and hybrid materials[48]. Solid-state pores have a higher stress tolerance, and are more readily fabricated than biological pores, although the structures are not well reproduced. Typically the solid-state pores are fabricated in a plane material. Nanocapillaries firstly used in patch clamp sensing is an exception. They are shaped like a tube with a tapered end, where is the nanosized opening. Nanocapillaries are usually made of glass or quartz. They are easy to make and cheap, as they do not require clean room facilities. Such capillaries can be combined with optical tweezers because their tapered shape and transparency do not interfere with the OT trap laser.

1.4 Optical tweezers combined with nanopores

To reduce nucleic acids translocation speeds as well as to study translocation kinetics people have thought of combining nanopores with optical tweezers. In this configuration, a trapped optical bead mimics a motor protein translocating DNA through a biological pore. Keyser et al were the first to successfully conduct experiments with nanopores integrated into optical tweezers setup[49] (Figure 1.6). They managed to measure the electrophoretic force on DNA translocating through a solid-state nanopore. In the experiment, voltage pulls the DNA attached to an optical bead through the pore. As a result, more of the DNA is pulled and it stretches between the pore and the bead, which then is pulled out of the optical trap centre.

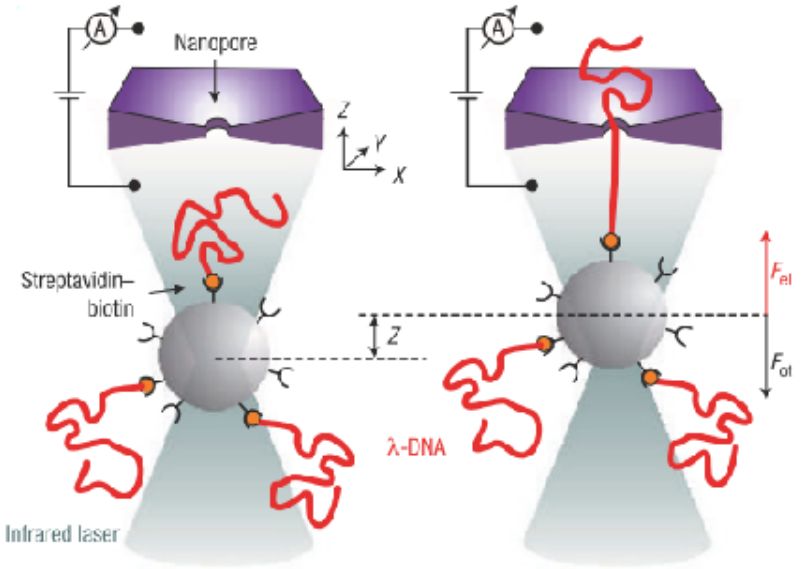

Figure 1.6: DNA translocation through a nanopore controlled by optical tweezers experiment. (a) Schematic of the experimental setup. In a salt solution, DNA-coated bead is optically trapped in close proximity to a solid-state nanopore. A positive voltage is applied to the back of the nanopore, driving the DNA through. Upon DNA translocation start the bead is pulled out of the optical trap centre with a certain distance, which allows calculating the electrophoretic force acting on the DNA. The figure is adapted from [49].

Later Keyser's group replaced 2D materials nanopores with glass capillaries[50, 51]. This geometrical change made the experiments easier to perform. First of all, the opening at the end of a capillary is readily found using a camera, whereas 2D nanopores cannot be directly located, as their size is smaller than the diffraction limit of light. Secondly, the optical trap does not interfere with a capillary as much as with a 2D pore due to its refraction index difference with the buffer. Furthermore, the fabrication of the glass capillaries and the sample cell is significantly easier and does not require clean room facilities.

With this combination, one can measure a protein position along a DNA[52] (Figure 1.7). In such experiment, the DNA enters the nanocapillary due to electrophoretic forces. The distance between the capillary and the optical bead is increased until the protein exits the pore. The optical trap is fixed, so the capillary is moved by a nanopositioning stage. Right before the protein approaches the capillary opening effective negative charge of the DNA-protein complex can direct it towards the capillary, and the DNA tension is partially released. The DNA is stretched again and the force increases.

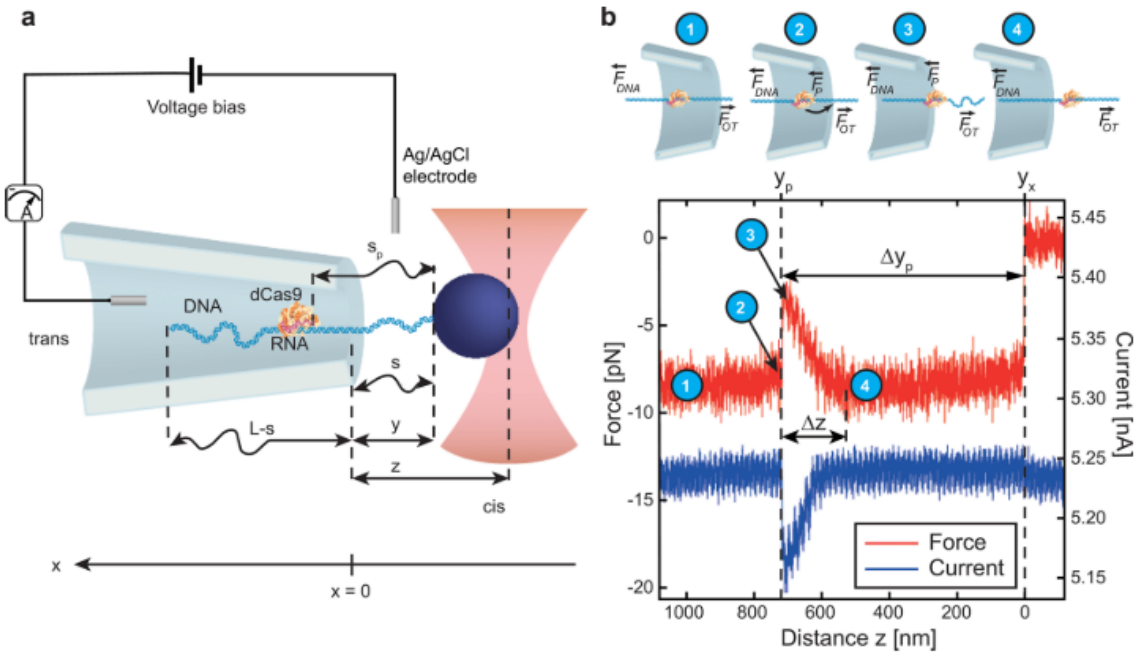

Figure 1.7: Protein detection along the length of the DNA. (a) Schematic of the experimental setup. Z marks the distance between the centre of the optical trap and the nanocapillary opening, while y is the distance between the capillary opening and the surface of the bead. L is the total length of the DNA, and s is the DNA length between the bead and the pore. The bead and protein distance is marked as s_p. (b) Typical force and current traces in relation to z. (1) Before the protein approaches the pore. The forces on DNA and the protein are comparable. (2) At the pore, the protein experiences larger force than the DNA. (3) Protein escapes the pore. DNA becomes less extended. (4) After the protein left the pore. DNA extension the same as before the protein approached the pore. When the protein is at the opening of the capillary the current changes and the force increases. The figure is adapted from [52].

Glass capillaries have their own disadvantages. Due to their conical shape, voltage application between the two chambers induces an electric field inside the capillaries' first 100-1000 nm from the aperture[53]. At a neutral pH, the surface charge of silica or glass capillaries is negative[54]. The salt solution screens the charges forming a several nanometer thick electric double layer at the glass surface. Locally, there is no charge neutrality. Therefore, upon application of an external electrical field, a nett force causes

fluid flow of the liquid (electroosmotic flow (EOF)) where the charge neutrality is not satisfied[55]. Moreover, when the DNA is in the capillary, the electrophoretic force, which is driving translocation, is opposed by the fluid induced drag flow. The EOF-induced drag force can effectively reduce the electrophoretic force on DNA 2 to 5 times[56–59]. At high salt concentrations the Debye layer is shorter, charge neutrality is satisfied in a bigger volume of electrolyte, and thus the electroosmotic force is lower[60] (Figure 1.8). With a reversed voltage (negative electrode in the trans channel), the EOF is low, and it is also diminished by the increase of the salt concentration. Therefore, EOF causes current rectification and asymetrical fluid flow, interfering with translocations. The drag force is inversely proportional to the size of the capillary[55]. Additionally, it was determined by the group of prof. Radenovic, that in the setup with nanocapillaries, the EOF induced drag force is larger than the electrophoretic force driving ssDNA into the capillary. For this reason, ssDNA cannot be used in OT experiments where a nanocapillary is used as a nanopore for single-molecule sensing.

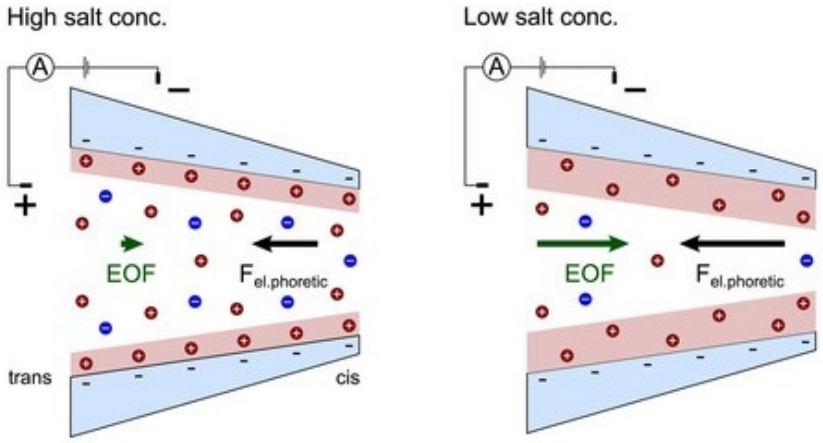

Figure 1.8: DNA translocations through a nanopore, dependence on ionic strength (salt concentration). Negative capillary walls charge is screened by positive ions forming an electrical double layer. Locally, the amount of cations is higher than anions. The cations driven towards the negative electrode forces the fluid to flow in the same direction. At lower salt concentrations, the charge neutrality is not satisfied in a larger volume. Therefore, the EOF induces fluid flow in a larger volume of the buffer and more strongly opposes the electrophoretic force driving the DNA to the capillary. The figure was adapted from [60] .

1.5 MspA porin

Biological nanopores are transmembrane protein channels. These pores are normally inserted into membranes, such as planar lipid bilayers, liposomes or block copolymers. Biopore availability and structure reproducibility facilitate single-molecule sensing. Using genetic engineering the pores can be readily modified[41]. The most widely used biopores are an exotoxin produced by *Staphylococcus aureus* a-Hemolysin[61], bacteriophage phi29 DNA packaging motor[62] and *Mycobacterium smegmatis* porin MspA[63] (Figure 1.9).

Due to MspA's unique geometrical structure containing a constriction comparable to the size of a single nucleotide, the pore applications in biophysics are beyond sequencing, e.g. for kinetic protein studies[64].

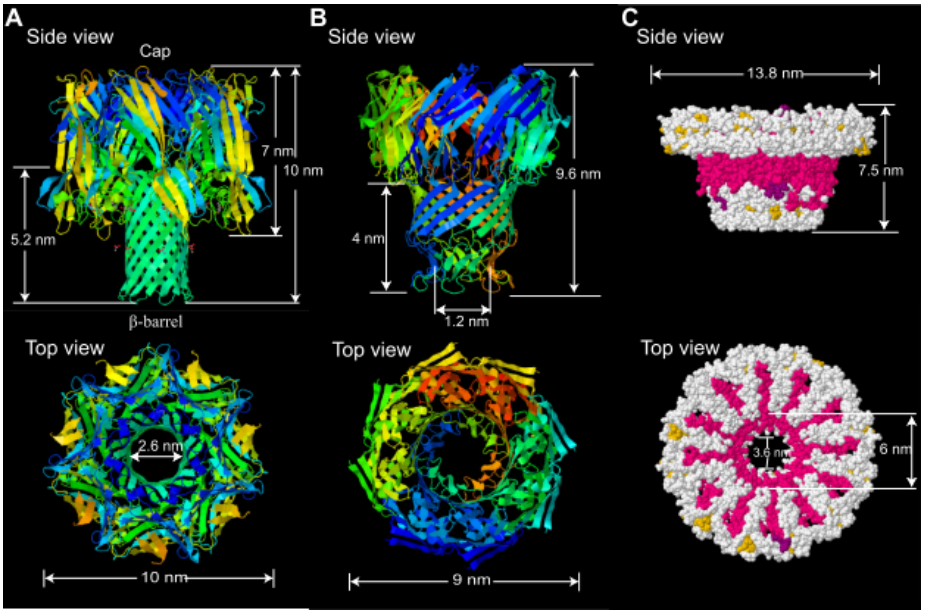

Figure 1.9: Side and top views of biopores. (A) Heptameric a-hemolysin. (B) Octameric MspA porin. (C) Dodecameric phi29. The figure is reproduced from [41].

A mutant of MspA - *Mycobacterium smegmatis* outer membrane protein is used in SPRNT as a nanopore. It is one of the most suitable nanopores for single-molecule analytical measurements due to its geometry and robustness. When the size of the pore matches well the analyzed structures size, the current drop is a significant amount of the total current (the current can be blocked by as much as 83 % [65]), making it easy to resolve. The MspA constriction length is 0.6 nm and its width - 1.2 nm, that matches well the size and spacing of single-stranded DNA nucleotides[63]. The biopore can withstand any pH from 2 to 14 and temperatures higher than 100 °C [66].

In 2008 Butler et al has demonstrated the first proof of ssDNA translocation through MspA, opening up an avenue for nanopore sequencing[63]. The area of the constriction is big enough only for one strand of DNA. A high density of negatively charged amino

acids in wild-type MspA repel DNA from entering the pore (Figure 1.10 A). In the DNA sequencing study, Butler et al used M1MspA, which is a D90N/D91N/D93N mutant, where negative charge containing interior aspartates were replaced with uncharged asparagines (Figure 1.10 b middle). MspA is an octamer, therefore 3 mutations in total change 24 amino acids in the pore. Another mutant D90N/D91N/D93N/ D118R/D134R/E139K (M2MspA) was made, where negatively-charged residues in the interior of the pore were replaced with positively-charged residues (Figure 1.10 b right). Both the mutants have smaller conductance than the wild-type porin, minimizing the possibility that a degraded lipid or other particles would spontaneously block the pore at higher voltages, and decrease the ionic current. This allows to use higher voltages and increase the probability of DNA entering the pore. In the same study it has been shown that DNA translocates through M2MspA approximately 5 times more often than through M1MspA at 180mV. Therefore, M2MspA mutations significantly facilitates DNA sequencing and SPRNT.

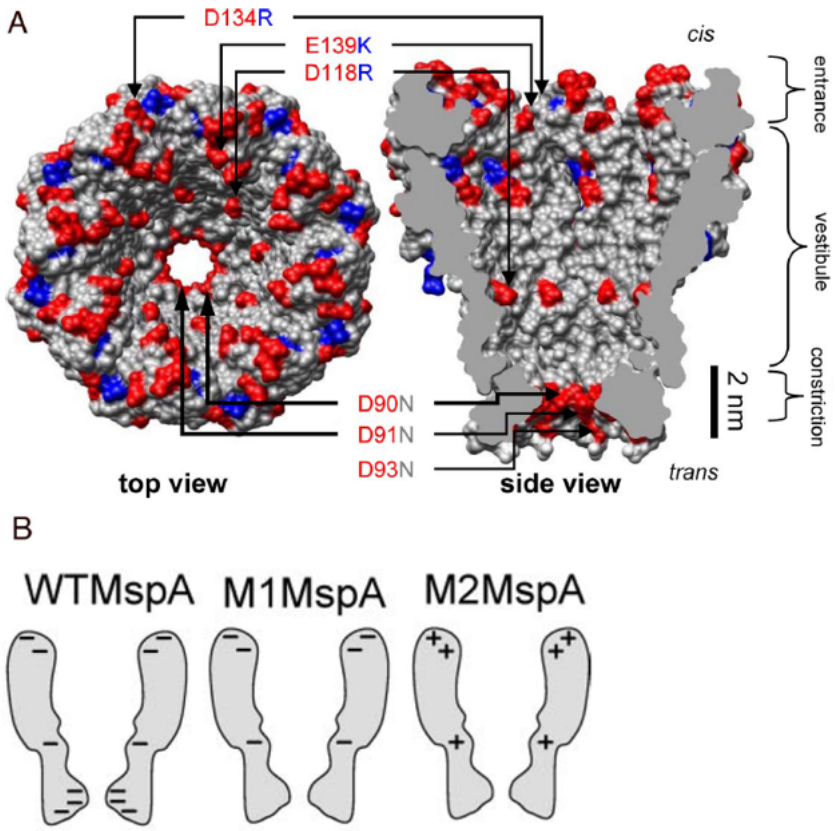

Figure 1.10: A) MspA and its mutants structure. At pH 8 negatively-charged aspartate and glutamate residues are coloured red, while positively-charged arginine and lysine residues are in blue. B) WTMspA – Wild-type MspA containing negative charge in its interior; M1MspA – mutant, where negatively-charged residues in the channel replaced with neutrally-charged ones. M2MspA – mutant, where the negatively-charged residues in M1MspA vestibule are replaced with positively-charged residues. Arrows and labels indicate the mutations. The figures were adapted from [64].

In 2012 Manrao et al showed that MspA can be used for DNA sequencing with single nucleotide resolution. Aforementioned demonstration of free translocations was not suitable for sequencing, as in this set-up DNA speed is 3 fold too fast to be able to discriminate specific to different nucleotides current changes from noise. While lower temperature and higher viscosity of the solution reduces translocation velocity, it reduces the current signal as well. To overcome this limitation, DNA polymerases of E. coli, bacteriophages T7 and phi29 DNAP helicase have been investigated as molecular motors, translocating DNA in a slow controllable manner[67]. Such proteins 'walks on DNA stepwise. When they are attached to DNA, one protein spontaneously locates itself above the pore, gradually passing-on the DNA to the nanopore. Due to the difference of the length of the pore constriction and the space between the nucleotides difference, each current change corresponded to the sequence of the four nucleotides in the proximity of the porin constriction at the time[67, 68] (Figure 1.11). Such resolution helps not only identify single nucleotides but also short homopolymer segments.

Due to the very high DNA sequencing resolution, MspA is used as a tool to study the kinetics of nucleic acid motor proteins. The new technique is called single-molecule picometer resolution nanopore tweezers (SPRNT). The measurements in SPRNT are essentially the same as in sequencing. For kinetic measurements, a known sequence of DNA is used. Each current level is associated with four nucleotides' size and the net charge they carry (Figure 1.11 a). Current data measured over time is allocated to the DNA sequence (Figure 1.11 b). A set of current levels (consensus set) for the motor protein used in translocations is produced. By interpolation of the current levels, a spline is obtained (Figure 1.11 c). Then another enzyme analyzed is used with the same sequence. The new enzyme current levels are then compared to the consensus set and the spline associated with the DNA sequence. This way sub-nucleotide step sizes can be deduced. The duration of the steps is known from the current measurements over time. Furthermore, the spline of the levels measured at 140 mV was found to match 180 mV measurement spline, and it is shifted by $\sim$0.3 nt (Figure 1.11 c, d). This means, that the current levels measured at 180 mV can be used to predict results at 140 mV (at different force acting on DNA)[65]. All this information helps to answer complicated questions, such as what DNA sequences make the protein pause or backstep[69].

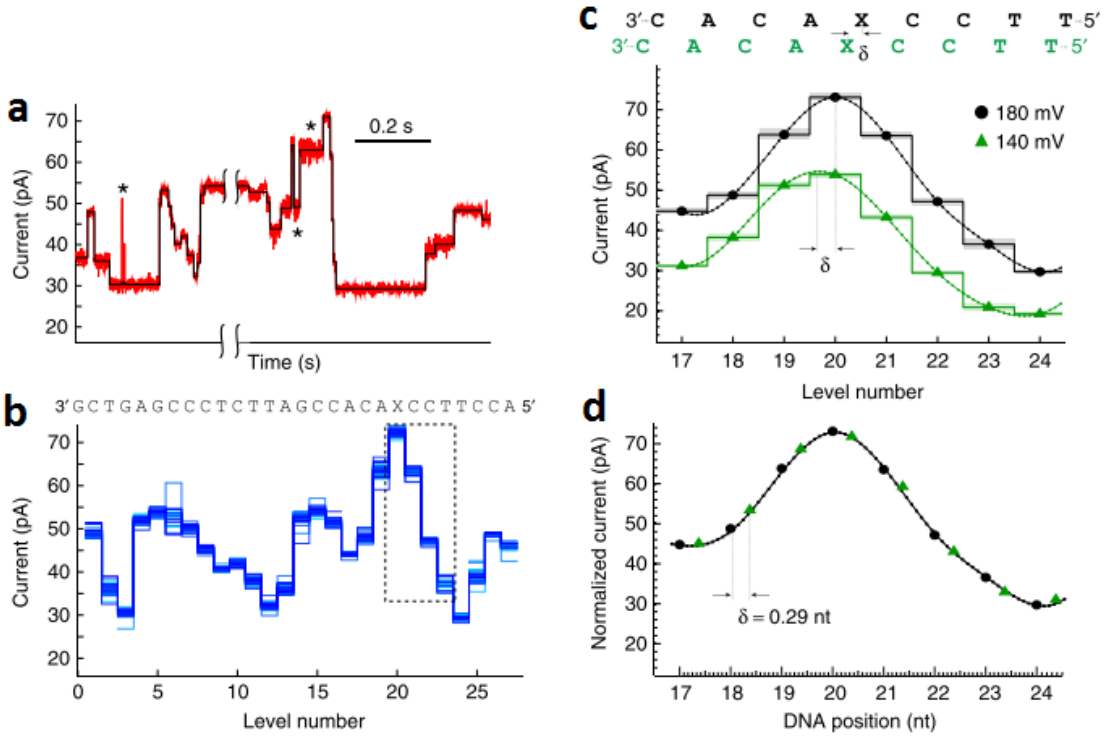

Figure 1.11: phi29 DNAP SPRNT measurements. (a) Current trace of phi29 DNAP translocated DNA. The black line is the mean currents of the levels. Asterisks mark the back-stepping of the enzyme. The time scale bar represents 0.2 s. (b) 31 measurements averaged current levels plotted against the corresponding DNA sequence. X is an abasic residue. (c) Spline interpolation of the current levels measured at 140 and 180 mV. A ∼0.29 nt shift between the current level splines taken at 180 and 140 mV is marked as . (d) Spline interpolation of the current levels recorded at 180 mV. The green triangles mark current levels observed at 140 mV, displaced by 0.29 nt. The figure was adapted from [65].

It is known that nucleic acid sequence controls the kinetics of some motor proteins[70]. Craig et al experimentally found that the ssDNA between the motor and the sequence measured at MspA constriction is 20 nt in standard SPRNT conditions[71]. Knowing the offset allows correlation of kinetics and DNA sequence in the motor. By repeatedly studying different DNA sequences with different motors, backstep and pausing probabilities at particular nucleotides arrangements can be found. Subsequent mutation of the DNA sequences, which were found to be causing back-step are performed, and the back-stepping probability dependence on the exact sequencing can be found (Figure 1.12). Backstep can be seen in the current trace as an additional event with the same values as the previous one, or in between them (if the enzyme made a step of a different length than going forwards). Longer than expected dwell times indicates pausing. SPRNT is the first tool allowing analyzis of sub-nucleotide enzyme steps in millisecond time scales along DNA.

Figure 1.12: Probability of a backstep correlated to DNA sequence in f the enzyme. 3 bases at position 9 were changed to cytosine in the following manner: (top) AGAC was mutated to ACAC, (middle) ACAC to ACCC, (bottom) ACCC to CCCC. Each sequential mutation lowered the backstepping probability compared to the original sequence. Whereas backstepping at other positions were not changed significantly. The figure was reproduced from [71].

Such resolution might seem impossible due to the Brownian motion, which causes significant changes in distance between the enzyme and the pore. Fortunately, these jumps happen at much higher frequency than the current is measured. SPRNT can precisely measure steps as small as 40 pm, with durations in the ms scale[65], making it the highest resolution single-molecule technique to study polymerases, helicases and translocases (Figure 1.13).

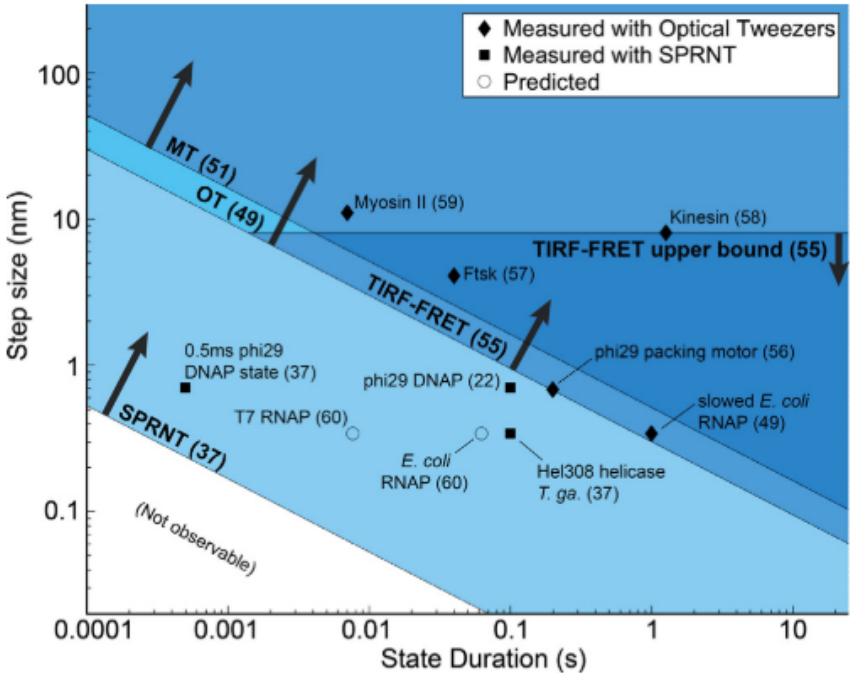

Figure 1.13: Spatio-temporal resolution comparison of SPRNT, OT and MT. The black diamonds represent average enzyme step sizes and durations resolved with optical tweezers. The circles indicate the estimated steps for other enzymes. The squares indicate the steps measured with SPRNT. The figure was reproduced from [64].

1.6 Lipid bilayer formation techniques

Channel-forming proteins are naturally found in lipid cell or nuclei membranes. For meaningful ion-channel current measurements, one has to embed them in a membrane separating two salt solution containing volumes. While, they can be inserted in different materials, such as block copolymers, lipid bilayers are the most widely used membranes for ionic current in channel protein experiments, such as DNA sequencing or protein positioning on DNA. Lipid membranes are formed on teflon tubes for SPRNT experiments[64]. Lipid membranes are good insulators, random ion flow through the membrane (not a channel) is improbable (low current leakage). It is is easy to detect the small current changes in the porins, as they are a large part of the total current passing. It also allows easy detection of the bilayer formation, by applying a voltage (usually around 200 mV), and measuring the current in the experimental cell. Moreover, there are many methods designed to form lipid membranes, which can be applicable for different experiment setups.

In one of the most simple techniques - Mueller-Rudin, the lipids are painted over a circular orifice[72]. In volatile organic solvents dissolved lipids are carefully swabbed across the hole until the bilayer is formed (Figure 1.14). By adjusting the solution the membrane thickness can be accommodated to fit different proteins' hydrophobic parts.

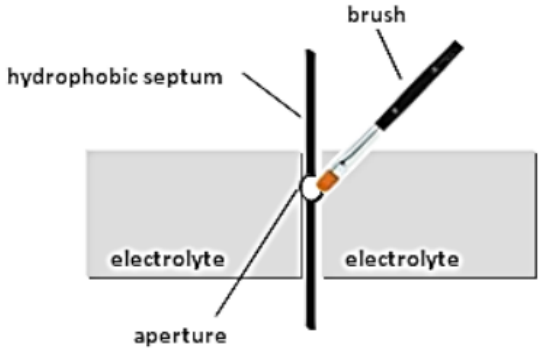

Figure 1.14: Schematic of a lipid painting technique. A lipid solution is painted over a teflon aperture immersed in an electrolyte. Teflon is hydrophobic, therefore it is energetically favourable for lipid bilayers to form on its surface. After painting, a bilayer forms spontaneously. The figure is adapted from [73].

This technique is also used in on a u-shaped teflon tube in SPRNT experimental setup[64] (Figure 1.15. The tube with outer diameter of 1mm, and the aperture of ∼20m is primed with lipids and filled with a buffer. A lipid goo is painted on the tube near the orifice. Bubbling over the aperture with a pipette forms a lipid bilayer, to which an MspA is inserted. The bilayers can be reformed more than 50 times.

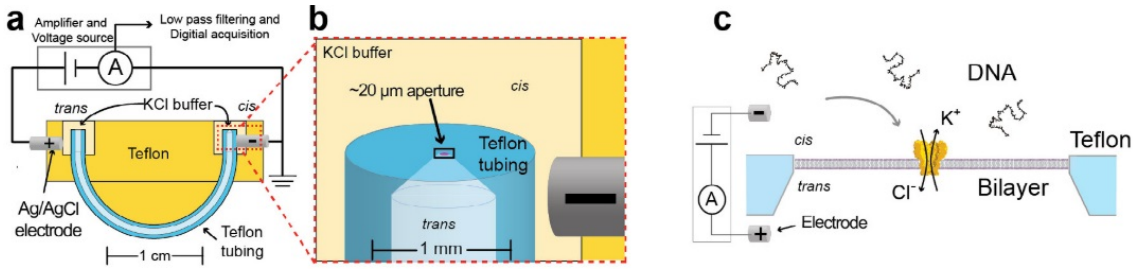

Figure 1.15: Schematic of the u-tube setup in SPRNT. The 1 mm diameter teflon the tube has a ∼20m orifice on which lipid bilayer is established. During the lipid painting, a large amount of lipid is left near the tube opening, on the wall. Lipid bilayers are easily formed by bubbling over the lipid residue. The figure was reproduced from [64].

Another simple technique is called the Montal and Mueller solvent-free method[74]. A droplet of lipid solution is transferred to a patched pipette filled with aqueous buffer and in contact with an aqueous surface. A lipid membrane is formed by applying suction at the back of the pipette[75]. In this case, the bilayer might be formed further back in the pipette (Figure 1.16). It is not ideal for an ion channel reconstitution, and experiments with optical tweezers, because the membrane is hardly accessible. For an ion channel protein to reconstitute into the lipid membrane, it must diffuse towards the bilayer. The capillary wall obstructs the pore from diffusing inside the capillary, and the likelihood of an insertion significantly decreases. Furthermore, it is practically inaccessible for optical tweezers experiments.

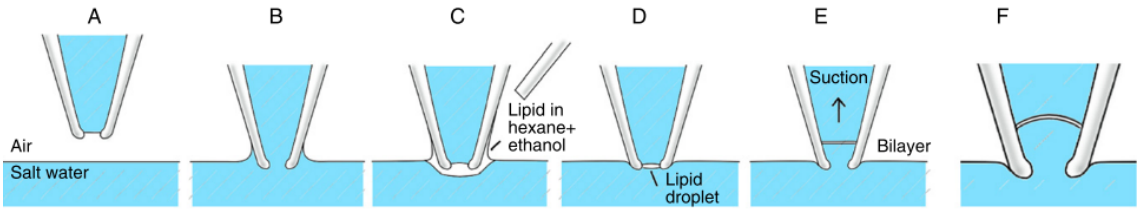

Figure 1.16: Schematic of Montal-Mueller patch-pipette technique. (A) A pipette is filled with an aqueous buffer. (B) The pipette is brought to close contact with an aqueous surface. (C) A drop of organic lipid solution is placed at the end of the pipette tip, sealing it. (D) The organic solvent evaporates. A lipid monolayer is left on the bath surface and a droplet is at the pipette tip. (E) A negative pressure is applied to the back of the pipette to thin out the lipid droplet into a bilayer. (F) A lipid bilayer is formed inside the pipette. The figure is adapted from [76].

Goll et al. have developed a method where the bilayers are formed on glass nanopipettes using giant unilamellar vesicles (GUV) containing channel proteins[77]. Here, a patch-clamp pipette is pointed by a micromanipulator towards a GUV in a solution. Then the pressure is slightly decreased at the back of the pipette, sucking in and rupturing the GUV and forming a lipid bilayer with a channel-protein (Figure 1.17). These bilayers are very stable - they can withstand 900 mV potentials for several hours. The membrane can be broken by increasing the pressure or voltage and reformed for more than 50 times. Their stability allows long-lasting experiments[77].

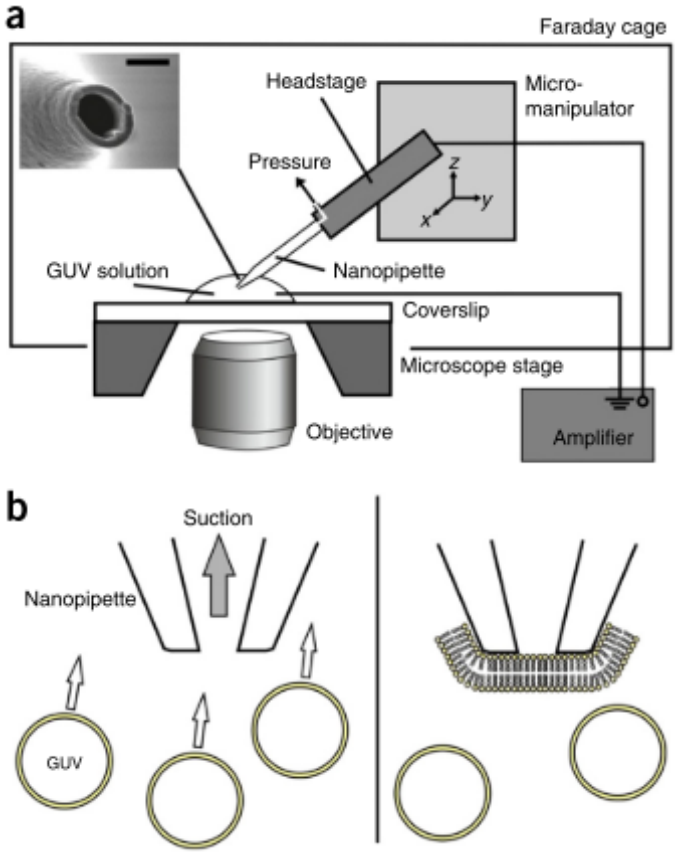

Figure 1.17: Schematics of a patch-clamp setup for lipid bilayers formation. (a) GUV solution is dropped on a coverslip above an inverse microscope. A nanopipette is dipped in the solution and positioned near a GUV. A negative pressure is applied at the back of the pipette rupturing the GUV and forming a lipid membrane. (b) Lipid bilayer formation on the pipette tip. The figure is adapted from [76].

Marin et al created a new method where the lipid seal is formed on a microchannel device made of solvent resistant and optically transparent photopolymer NOA81[78]. This configuration is optically transparent and can be combined with optical tweezers. Firstly, the microchannels are filled with organic solvent using pressure pump. Then an aqueous lipid solution is flowed to the channels. The organic phase is thinned out near the aperture connecting the microchannels. The lipids leave the buffer dissolving in the organic solvent and forming a bilayer (Figure 1.18). 1,2-diphytanoyl-sn-glycero-3-phosphocholine lipid (DPhPC) membrane formation was observed in ∼80% of the apertures. This highly reproducible method was successfully used for single -hemolysin insertions. The ionic currents of the channel were in a good agreement with previous studies, the flow cell and the lipid membrane formation technique did not change the behaviour of the porin -hemolysin[78]. Although, it is not known whether these organic solvents would change MspA behaviour.

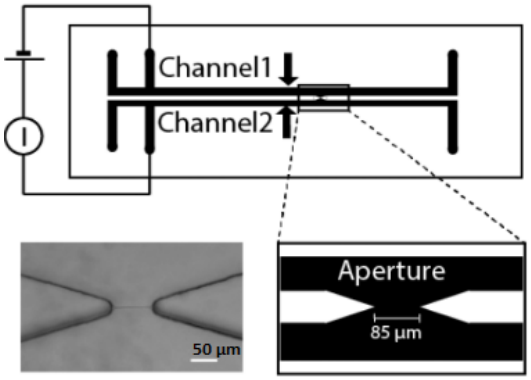

Figure 1.18: Schematic of NOA81 microfluidic device. Top view of the microchannels. Bottom left is a bright field image of a lipid membrane. The figure is adapted from [78].

Materials and methods 2

In our study we adapted the Mueller-Rudin technique. This method can be used on simple setups, there is no need to fabricate a complicated microfluidic cell. Furthermore, the lipids are dissolved in the same solvent (hexadecane), as in the paint used on teflon tubes in SPRNT experiments[64]. This eliminates unknown effects of different solvents.

2.1 Materials

M2MspA proteins were ordered from Genescript. 1,2-diphytanoyl-sn-glycero-3-phosphocholine (DphPC) lipid was supplied from Avanti Polar Lipids. All the dry compounds for buffers and solvents were ordered from Millipore Sigma.

2.2 DNA synthesis and preparation for optical tweezers experiments

Ligation of biotin containing oligomer (77) to one of Lambda DNA cohesive ends (12 bases). Lambda DNA and biotinylated oligomer (1:10) were annealed at 65 °C for 1h, then the temperature was ramped down to 25 °C at 1,2 °C/5 min. The annealing mixture was further used to ligate with T4 DNA ligase at 16C overnight. The enzyme was inactivated at 65 °C for 10min. The oligonucleotide excess was removed by filtration through a spin column (Clontech CHROMA SPIN TE +1000).

M13mp18 single-stranded DNA annealing with an oligo (M13HindIII) to prepare a double-stranded HindIII site for enzymatic restriction. M13mp18 plasmid was annealed with the oligomer (1:25) by incubating the reaction mix at 95 °C for 30 min, then the temperature was lowered by 1 degree per minute to 25 °C. The annealing product of M13mp18 with M13HindIII was restricted at the HindIII site at 37 °C for 1h. The enzyme was inactivated at 80 °C for 20 min. Linearized M13mp18 DNA was purified using NucleoSpin Extract II kit (MACHEREY-NAGEL).

Biotinylated Lambda (Lambda-biot) and linearized M13 (ratio 1:1.1) ligation using an oligomer (LAMBDAM13OK). The components were firstly annealed at 65 °C for 1h ramping down the temperature to 25 °C at 1.2 °C/2 min. Ligation using T4 DNA ligase at 16 °C overnight followed. The enzyme was then inactivated at 65C for 10min.

The final construct PCR confirmation. The experiment was performed using Phusion high fidelity PCR master mix and RevM13Lambda, FwM13Lambda primers. The PCR was set to 94 °C for 5 min, 30 cycles: 30 s at 94 °C, 1 min to 63 °C, 1 min at 72 °C; and 7 min at 72 °C.

DNA attachment to an optical bead. The DNA (∼100 ng) was incubated at 37 °C for 30 min, 250 rpm with 10 L of 3 m streptavidin-coated polystyrene beads (Bangs Laboratories), resuspended in 0.5 mL of 400 mM KCl, 10 mM MgCl2 and 10 mM HEPES buffer (pH 8.0). The resuspended beads were immediately placed on ice, and kept there. The new beads were prepared each day to avoid using sheared DNA.

Table 2.1: List of oligomers for the DNA construct synthesis

Name	Sequence
77	5'-GGG CGG CGA CCT T-3'-Biot
M13HindIII	5'-GTG CCA AGC TTG CAT G-3'
LAMBDAM13OK	P-5'-AGG TCG CCG CCC TGC ATG CCT GCA GGT CGA CTC TAG AGG ATC CCC-3'
RevM13Lambda	5'-GGC GTT CGT ACT CAA TAG TTC CTG GC-3'
FwM13Lambda	5'-GGG TGA TGG TTC ACG TAG TGG GCC-3'

Here Biot stands for Biotin and P for phosphorylation.

2.3 Fluidic cell fabrication

Capillary fabrication. A P-2000 laser-assited puller (Sutter instruments) was used to pull fused silica (360 m OD, 200 m ID) capillaries. To make the opening in the range of 2.5 to 8 m a pulling program was used with the following settings: Heat = 490, Filament = 4, Velocity = 10, Delay = 145, Pull = 160 The microcapillaries were images under scanning electron microscope (SEM) Merlin (Zeiss) (Figure 2.1).

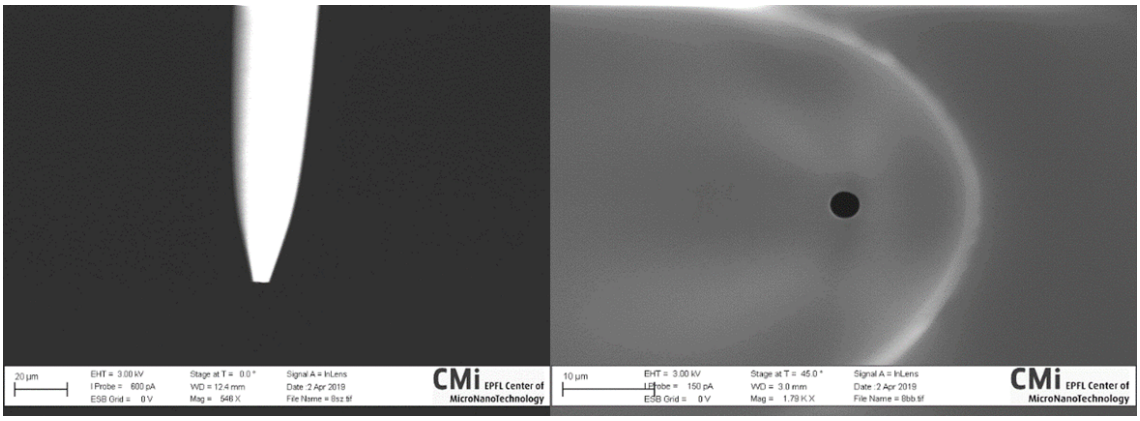

Figure 2.1: SEM images of a capillary. Left - side view, right - front view.

Silanization. For a more hydrophobic surface of the capillaries, a monolayer of a silane with exposed cyano group was formed. The capillaries were placed on a thick glass slide using double sticky tape. For the more effective treatment, the surfaces were prepared by oxygen plasma cleaning at 50 W for 10 min. Immediately after plasma cleaning, capillaries side facing downwards the glass slide was placed in a desiccator, over a glass petri dish containing several drops of 3-cyanopropyldimethylchlorosilane ($Cl(CH_3)_2Si$-$(CH)_3CN$, Gelest, Inc.). Vacuum was then applied for 10 min.

Ag/AgCl electrode preparation. Silver wires were chlorinated in 4M KCl at ∼1.5 V for ∼20 min or more with a negative Ag electrode.

Cis chamber fabrication. For the fluidic cell, PDMS (polydimethylsiloxane) was moulded forming a frame for a cis chamber. PDMS was prepared by mixing curing agent and precursor at 1:10 mass ratio. The mixture was then degassed in a desiccator to remove the bubbles. Then the PDMS was moulded and cured at 130C. The moulds were washed by ultrasonication in isopropanol and then milliQ water for 15 min each to remove any contaminants which would increase current leakage through the chambers. Finally, the clean PDMS was dried at 80C for 2 hours. **Sample cell assembly.** A capillary was placed in a PDMS wall indentation in a way, that the narrowest side of the capillary was facing the cis chamber, while the back end was outside the cell. The PDMS walls were painted with a layer of liquid PDMS. An Ag/AgCl wire was placed with its chlorinated end inside the cell. A standard 1 m thick microscopy coverslip was placed over the cell, flipped and heated at 130C for a few minutes to seal the fluidic cell. Then additional PDMS was dropped above the middle of capillary outside the cell, to secure it to the glass slide.

2.4 Experimental setup

IV curve measurements. An axopatch 200B ultra low noise patch clamp amplifier (Molecular Devices) was used to apply a voltage and measure the current. The flow cells trans chambers were connected by Ag/AgCl wires to the amplifier, while the cis chambers were grounded. The electrical circuit was located inside a Faraday cage, with the ground connection of Axopatch connected to the Faraday cage. Proper connections allow the removal of all ambient electrical noise and pushing the noise in the experiments to the limit of the patch clamp amplifier used. The experiment was controlled and data was aquired using a custom LabView program. The data was plotted using Matlab.

OT and capillary flow cell combination. In the setup, a flow cell was placed on piezoelectric nanopositioning stage (Mad City Laboratories). An x, y, z macromanipulation stage allowed rough adjustment of the capillary focus and position. A joystick was used to control the nanopositioning stage in order to move the bead aligning it with the capillary. The cell was illuminated from above using a white light source (Thorlabs) and visualized by a CCD camera (Thorlabs). Optical beads were trapped using a Nd:YVO4 solid-state laser (Coherent, 2.5 W, = 1064 nm). A telescope (3x) was used to expand the laser beam, which then had to go through a water immersion microscope objective (Nikon, 60x, 1.2 NA) before hitting the specimen. Then it was collected by a condenser (Olympus, 0.8 NA) and projected onto a photosensitive detector (PSD) (Pacific Silicon Sensor Inc.). The Ag/AgCl electrode from the trans chamber was connected to an Axopatch 200B ultra low noise patch clamp amplifier (Molecular Devices), which was used to apply an electric field and measure the current in the cell. The wire coming from the cis compartment was grounded to the aluminium Faraday cage built around the nanopositioning stage, amplifier, condenser and PSD. All protruding metallic optical components were connected to the Faraday cage to ensure no noise transmission inside the cage. A custom LabVIEW program was used to view the CCD transmitted images, joystick control, force and current recording (Figure 2.3).

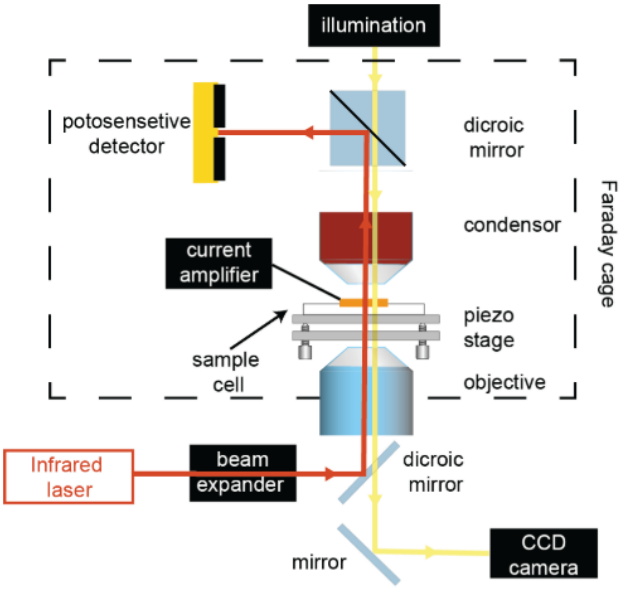

Figure 2.2: Schematic of the setup for optical tweezers and capillaries combination. The image was reconstructed from [79].

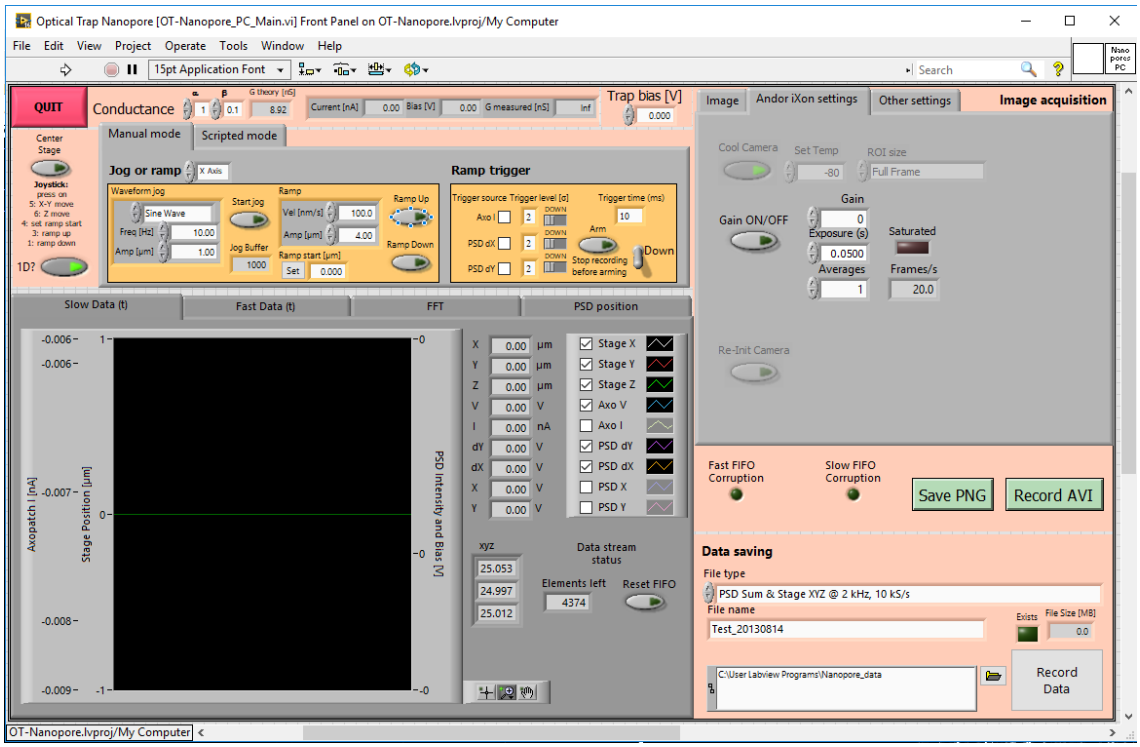

Figure 2.3: A screenshot of the LabView program used in the OT experiment.

Results and discussions 3

In our experimental design, capillaries with a few micrometres diameter apertures are used. Capillaries in the nanometer range are hard to fill with buffer, and also they break more easily. Bigger apertures also allow to form bigger membranes, and MspA reconstitution is facilitated. An optical bead with a several micrometre long DNA is trapped by optical tweezers and placed close to the capillary aperture. Positive voltage in the trans channel pulls the DNA in and through the pore (Figure 3.1). The force acting on the DNA is obtained from the bead displacement from the optical trap.

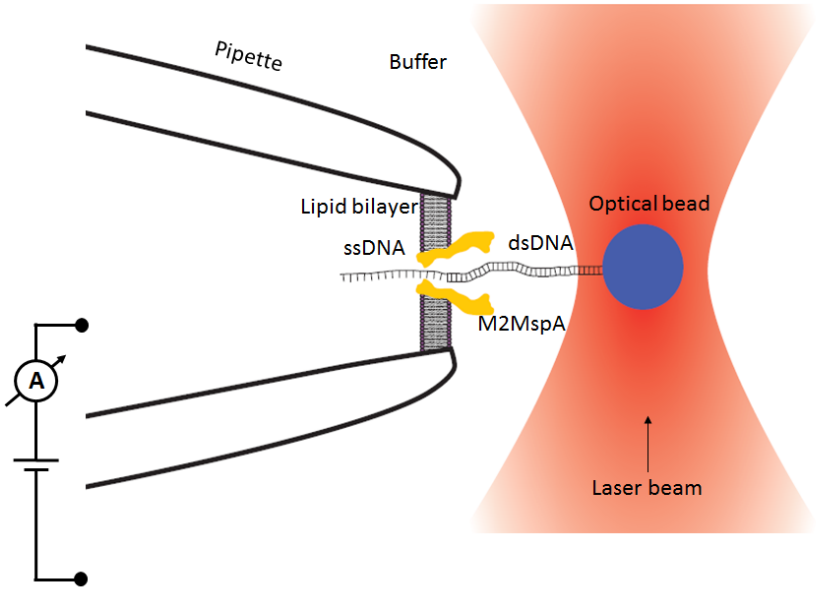

Figure 3.1: Schematic of the force on DNA translocating through MspA pore measurement experimental setup. A flow cell with a capillary connecting trans and cis channels is filled with buffer. Positive 180 mV voltage is applied to the trans channel. A lipid bilayer is established at the capillary orifice. An MspA pore is reconstituted to the lipid membrane. An optical bead with attached DNA molecules is trapped by the optical tweezers. The DNA translocates through the pore and displaces the bead from the optical trap.

In this chapter, we will discuss the development of the flow cell, lipid bilayer formation technique and the DNA construct needed to perform the experiment.

3.1 Silanization

The exposed -OH groups make the glass surface hydrophilic. While it helps to fill the capillary, it is an unfavourable surface for lipid bilayers. To make the lipid formation on the capillaries easier, we silanized them with 3-cyanopropyldimethylchlorosilane. The silane makes a monolayer with exposed cyano- groups leading to intermediate hydrophobicity. This compound has been used to coat quartz and glass nanopore membranes by White group[80] (Figure 3.2).

Figure 3.2: Schematic of a DPhPC bilayer across the opening of a quartz nanopore membrane silanized with 3-cyanopropyldimethylchlorosilane. The figure was reconstructed from [80].

While in the study, the technique was complicated and lasted more than a day, we were able to simplify it to a 20 min procedure. A glass slide was treated the same way as the capillaries to observe the wetting contact angle changes. The contact angle of a water drop with a surface is a characteristic describing surface wettability. A solid surface having a high affinity to water, causes the water to spread on the surface more. The droplet is almost flat, thus the contact angle is low. Hydrophobic surfaces, on the other hand, make water drops form more spherical shapes, with a high contact angle. Surfaces with a contact angle higher than 90C are considered hydrophobic, and more attracted to other hydrophobic materials, such as oils. From figure 3.3 we can see that the water droplet on the silanized surface has a significantly higher contact angle than the same volume drop on the untreated glass slide. Therefore, the silanization made the glass surface more hydrophobic.

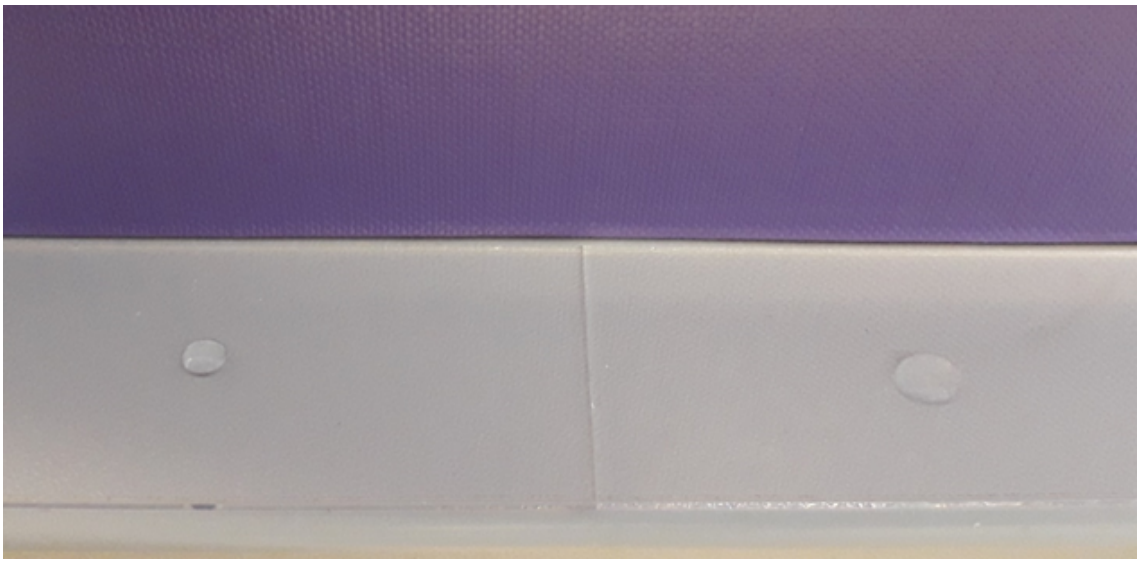

Figure 3.3: Image of the silanization effect on glass slides. Left - a glass slide silanized with 3-cyanopropyldimethylchlorosilane, right - untreated slide. Both the water drops are 10 L.

3.2 Trans chamber design

To unclog the lipids and fill the capillary with the buffer we needed to find a way to apply pressure at the back. Initially, we had the cell with two rectangular chambers connected by a capillary. This way we were trying to fill the capillary by gently pressing the trans chamber with another flat piece of PDMS. It was good enough to fill and unclog the capillary, but over time leaks would form between the PDMS and the coverslip. To overcome the issue, we connected a 1 mL syringe to the capillary through a series of pipette tips with cut ends and a flexible tube (Figure 3.4). The plunger was assembled with a silver wire to apply the potential.

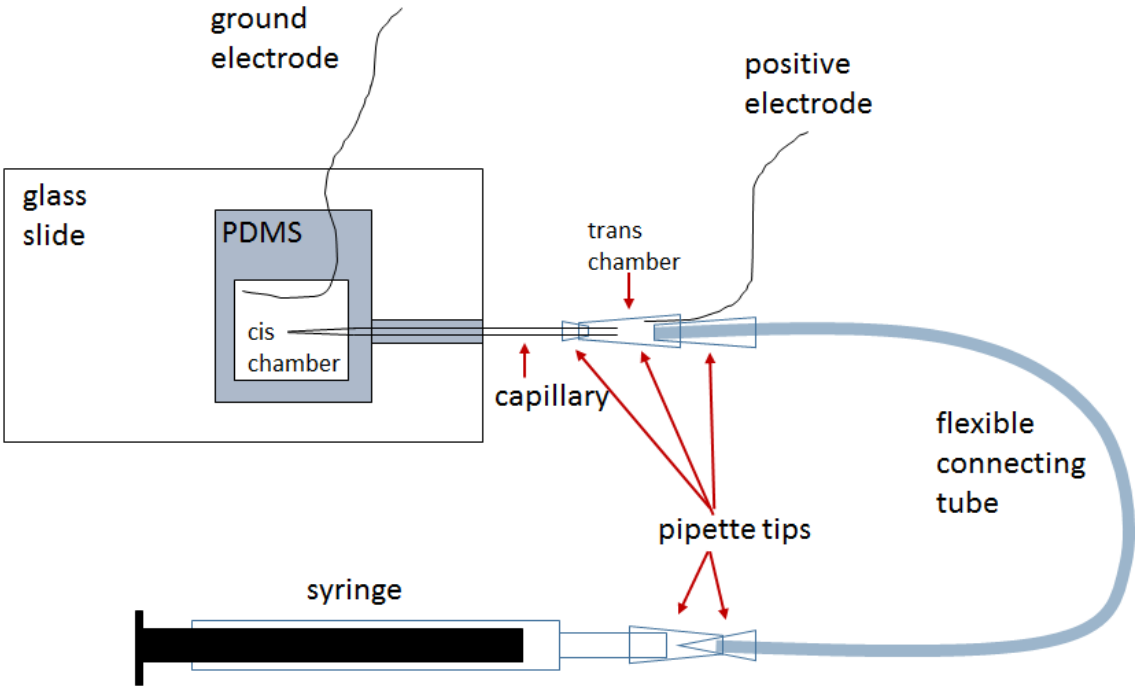

Figure 3.4: Schematic of the flow cell connected to a syringe for pressure application.

The plunger made experiments easier. Although, even without pushing the syringe plunger, it would apply pressure to the capillary. Therefore, during the painting process, it had to be disconnected after unclogging, leaving only a couple of pipette tips with the wire.

3.3 Lipid bilayer formation

The lipid bilayer formation on teflon u-pucks procedure was adapted to our capillaries. As in the u-puck setup, the capillary tips in the fluidic cells were primed with lipids for a better lipid paint adhesion. The DphPC lipid for priming and painting was prepared as in [64]. 0.2 mg of dried DphPC lipid is dissolved in $\sim$ 66 mg of hexane. Half the microliter is dropped on the capillary end. After 10 minutes, another portion is applied. Extra care must be taken not to allow any contact of plastic with hexane, which would lead to contamination. With time oxidation of the lipid prime tend to lead to short-lived bilayers. Therefore the capillaries are primed not more than 3 days before the planned experiments.

In order not to break the capillary during painting, it has to be visualized using a camera or a microscope. The capillarry is filled with buffer using the plunger, then the cis well is filled as well. Open capillary current trace indicates when the capillary is filled and no bubbles are obstructing the ion flow in the capillary.

After priming, the paint is prepared, by mixing a dried lipid with hexadecane on a glass slide to the right consistency. The paint is mixed using 'brushes' made of cut pipette tips in a shape resembling fountain pen. Before every use the brushes must be cleaned with ethanol and water, leaving no ethanol residue which brakes the bilayers. The consistency must be similar to the toothpaste's. Too much hexadecane leads to clogging, while too little causes short-lived leaky bilayers.

The lipid-oil mixture is then gently swabbed on the capillary opening till clogging is observed by significant current depression. The clog is removed by applying a little bit of pressure at the back of the capillary. Finally, a lipid bilayer is formed by pipetting $\sim$5 L bubble over the orifice. No current is observed when the bilayer is intact. If no pore insertions are observed, the capillary might be clogged. This can be checked by 'zapping' the bilayer with 1 V 5 s pulse. If a bilayer was broken it can be reformed a few times more just by bubbling over the capillary (Figure 3.5). Because the glass walls around the pore are very thin in comparison with SPRNT's u-tube, not a lot of lipid residue is left there. This reduces the clogging probability and the number of times the bilayer can be reformed on a capillary in comparison to a teflon tube significantly. It decreases the optical tweezers experiment success a lot. Therefore, the painting technique or the flow cell setup is not ideal and needs further modifications.

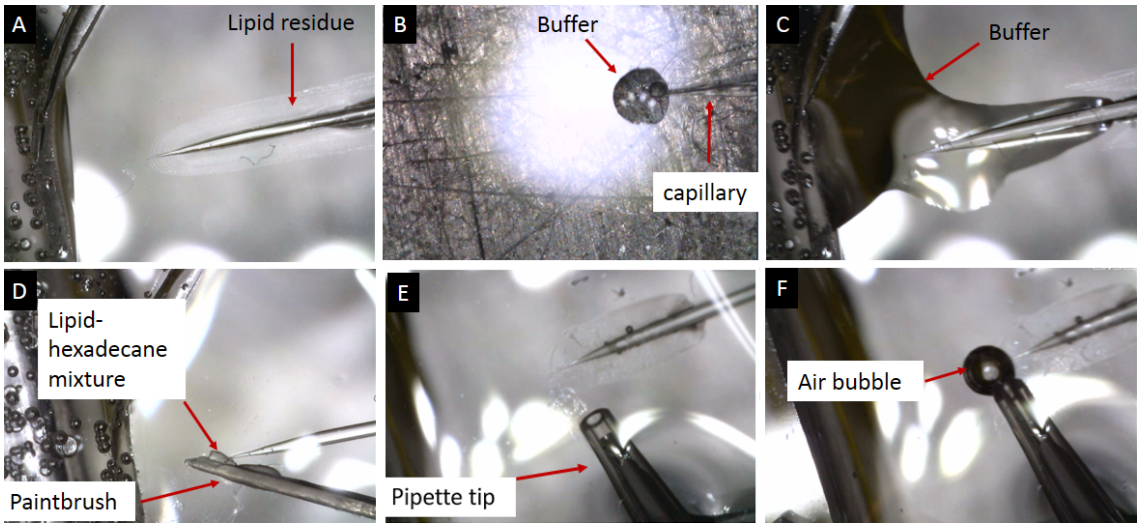

Figure 3.5: Image sequence of lipid bilayer formation on a capillary. (A) Capillary is primed with lipids. (B) The capillary is filled with buffer from the back. (c) The chamber is filled with the same buffer. (D) The lipid-hexane mixture is swabbed on the capillary aperture clogging it. (E) A pipette aimed at the capillary orifice. (F) A bubble is formed and retracted over the opening forming a lipid membrane.

Although the painting technique is working, it would be reasonable to explore different lipid membrane formation approaches.

3.4 MspA insertion into a lipid membrane

MspA insertion in a lipid bilayer is a stochastic process. We found it to be enough to add 1 L of 1 g/ml buffer containing MspA stabilized with 0.1% OPOE detergent to the cis chamber. It is then mixed in the buffer by pipetting. A pore usually inserts after waiting for a few minutes. It can be observed as a current change from 0 to ∼160 pA at 180 mV (Figure 3.6). Because of the way proteins diffuses in the chamber, one pore insertion is usually quickly followed by multiple other pores. The buffer in the cis chamber must then be quickly perfused to avoid multiple insertions. Before perfusion, the syringes are grounded to avoid breaking the membrane from a high voltage electrostatic discharge which might build up. If a wire is touched or the buffer volume gets too low, that also breaks the lipid membrane.

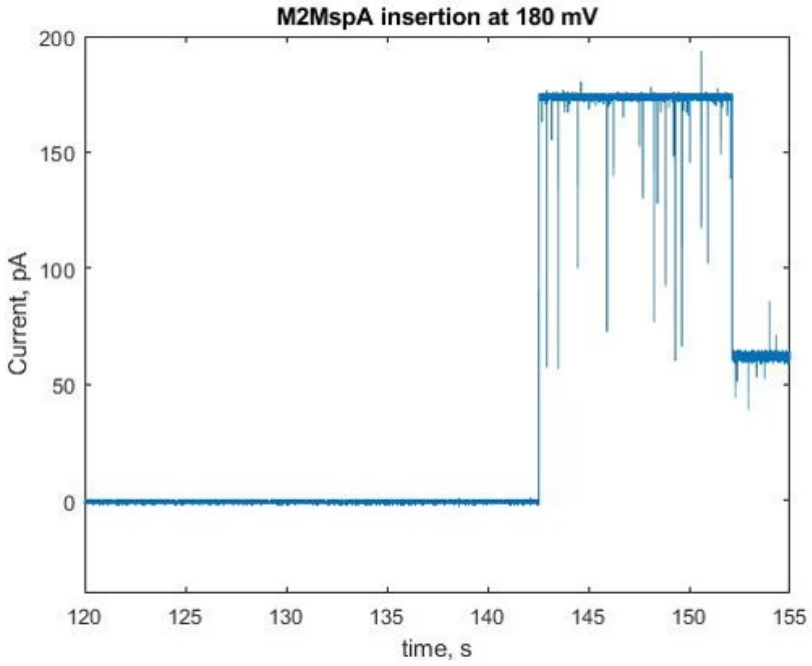

Figure 3.6: A current trace of M2MspA pore insertion to a lipid bilayer. At 143rd second, current jumps to 160 pA, a characteristic open M2MspA current at 180 mV. At 152 second, the current drops due to a spontaneous blockade.

Even without adding DNA to the flow cell, the pores tend to be partially blocked over time, leading to a decrease of the ionic current (Figure 3.6). This phenomenon is called a spontaneous blockade. If a pore does not open spontaneously, it can be done by flipping the voltage. Although, due to fewer negative charges in the channel close to the constriction, M2MspA mutant is blocked less frequently than wt-MspA [63]. Thus, higher voltages can be used for DNA translocations, significantly increasing the probability of DNA entering the pore.

Often a pore spontaneously leaves the membrane. If the buffer was already exchanged, it complicates the experiment, and many steps have to be repeated. As a compromise,

one can omit the difficult step and let multiple pores insert, sacrificing the current data. If multiple DNA molecules are drawn into the pores, one can possibly see the step-wise increase in the force trace. This way the difference between the steps, would be equal to the force acting on one DNA. Although, it is harder to recognize the DNA insertion only by the force trace, without the current data.

3.5 Current-voltage characteristics

M2MspA was characterized by current-voltage measurements in the flow cell developed in this study and in a teflon puck used in SPRNT measurements [64, 81]. The results showed the same conductive behaviour of the pore between the two setups (Figure 3.7). Consequentially, we can assume that the characteristics of capillaries, such as a large electroosmotic flow and current reactification do not influence either the ionic conductance of the pore or its stability.

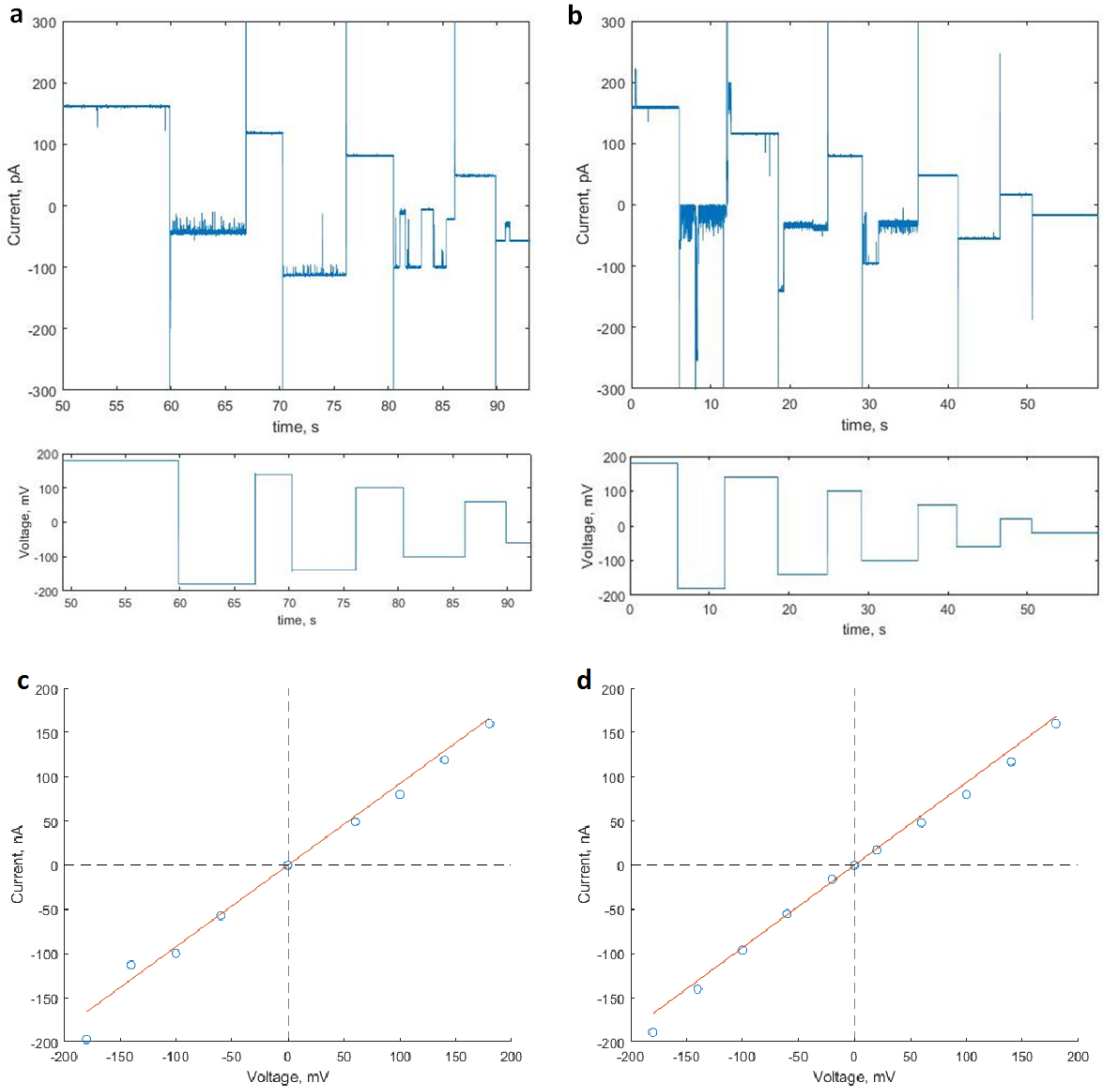

Figure 3.7: Current-voltage characteristics of M2MspA pore reconstituted in lipid bilayer on a capillary (a) and on a teflon tube (b). Top - measured current, bottom - applied voltage. (c, d) the I-V curves of M2MspA on a capillary and a teflon tube, respectively. At negative voltages, we plotted the current values right before gating started. The data fitting lines are drawn in red.

From the figure 3.7 we can observe current values obeying Ohm's law, but an application of a negative voltage shows a different pattern. At low negative voltages, from time to time the pore conductance decreases and jumps back again. At very high negative voltage (>100 mV), the current obeying Ohm's law lasts only a few milliseconds before stabilizing at the blocked state (Figure 3.8). This behaviour is called "gating". It has been observed in many biological pores, including wild- type[82] and mutant[83] MspA. Compared to wt-MspA[82](Figure 3.9), M2MspA gating is less pronounced in lower voltages. Voltage gating occurring in a strong electric field is supposedly caused by conformational changes of a biological pore, restricting ionic conductance in the channel. It has been found to be a common feature with other -barrel porins, i. e. -hemolysin, which do not have any other structural similarities with MspA. By studying the protein mutated at different sites, it has indeed been confirmed that a -barrel contributes the most to the change in conductance, although the exact mechanism is not known[83, 84]. Naturally, the pores which are reconstituted in a lipid bilayer backwards are gating when the positive voltages are applied to the trans channel, therefore they cannot be used in SPRNT or sequencing experiments.

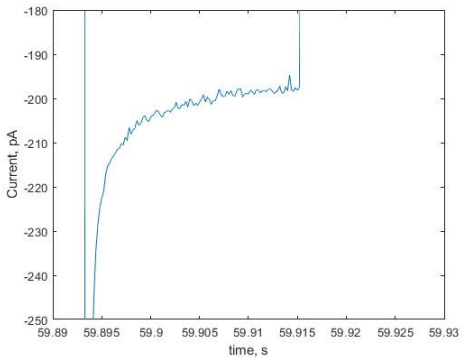

Figure 3.8: A closeup of M2MspA in the capillary setup current before starting to gate measured at -180 mV. The pore in its open state stays for approximately 10 ms.

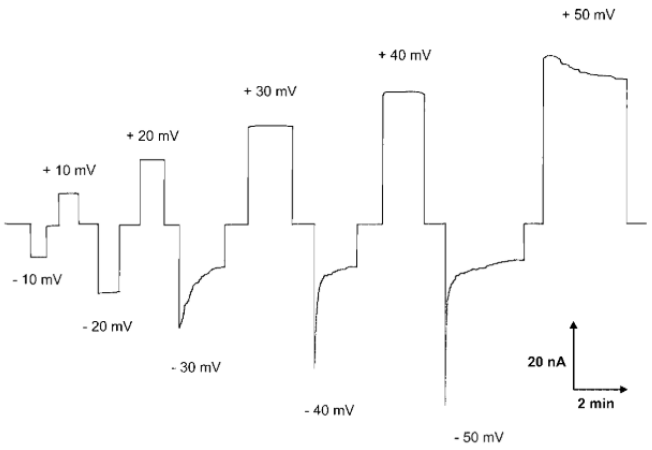

Figure 3.9: Wild-type MspA in DiphPC lipid membrane current-voltage measurement results. The figure was reproduced from[82] .

3.6 DNA construct design

For MspA's combination with optical tweezers, we needed to design a suitable DNA construct. While only single-stranded nucleic acids can fit in MspA's constriction, ssDNA is not stiff enough and has low volume exclusion. Having only ssDNA would mean that most of the DNA on an optical particle would be collapsed into a coiled structure, and DNA insertion into the pore would be improbable. To ensure that the DNA attached to an optical bead is long enough to reach the pore, we chose a 48,5 kb (∼16.5 m) long Lambda DNA. To which we ligated a linearized M13mp18 single-stranded plasmid. M13mp18 is 7249 bases long and, although such length is much longer than the pore itself, we chose it to be sure that only ssDNA reaches the constriction of the pore. In the vestibule of the pore, the electrophoretic force is strong enough to unwind the dsDNA. In that case, DNA would experience different magnitude of force than in SPRNT.
We used streptavidin coated beads to ensure specific attachment to the DNA construct. Therefore, we also needed biotin at the end of Lambda. Lambda is a bacteriophage. Its genome itself encodes an enzyme terminase which specifically cut the circular lambda DNA, leaving 5' strand overhangs by 12 bases at each site (cos sites). Naturally, we ligated an oligomer with an extra base and biotin at the end to one of the cos sites (Figure 3.10 a).
Next step was to linearize M13mp18. Most enzymes cut double-stranded DNA. For this reason, we annealed a complementary oligomer to a single HindIII site on the plasmid (Figure 3.10 b). Several bases to each side of the restriction side were added, for more effective hybridization, and to leave enough space for the restriction enzyme. After the annealing, the DNA is cut. At this point on each end of the DNA there is an oligomer residue, where 6 bp are hybridized. It is short enough to detach from M13mp18 at room temperature. The construct was confirmed by PCR amplification of the final construct, where one primer was complementary to a part of M13mp18 and the other to the overhung Lambda strand. While the reaction confirmed the presence of the correct product, it does not provide any quantitative data.
Finally, Lambda and M13mp18 are ligated through a linker, which 12 bases are complementary to a Lambda cos site, and the other 33 - to the 3' end of linearized M13 (Figure 3.10 c). Every day, before the experiments, the DNA construct was attached to the optical beads (Figure 3.10 d).

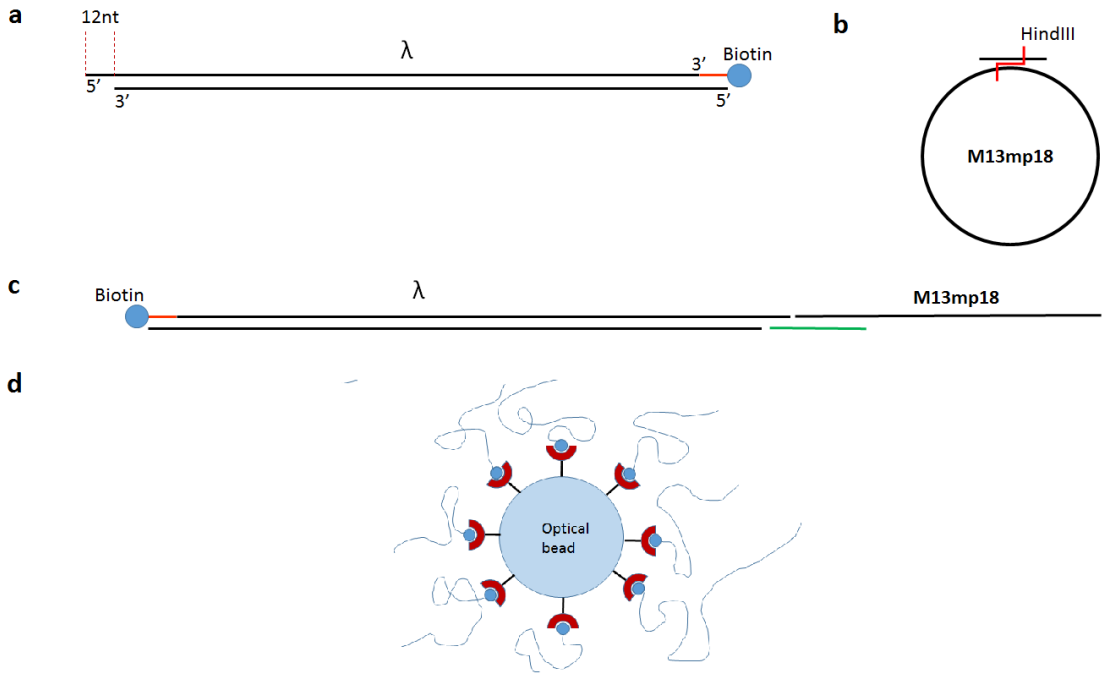

Figure 3.10: Schematics of DNA construct synthesis and attachment to optical beads. (a) Lambda DNA biotinylation. (b) M13mp18 linearization. (c) Lambda and M13mp18 ligation. The green strand depicts the linker. (d) DNA construct attachment to an optical bead. Red figures represent streptavidin, the blue lines - DNA construct.

3.7 Force measurement

We attempted to measure the force in the capillary setup several times. This experiment involves multiple steps, which set limitations. Firstly, we managed to successfully form lipid membranes sealing the capillary end. The bilayer stability was tested by moving the optical trap laser beam across the capillary. Fortunately, the laser heat did not affect the bilayers. Secondly, we were able to get MspA insertions. But getting a single pore in the bilayer was complicated, often the pore would leave too soon. As a compromise, we decided to let multiple pores to insert.
After pores were reconstituted in the membrane, the DNA coated beads were injected into the cis chamber. The beads were readily captured by optical tweezers and brought to the close proximity within the capillary opening (Figure 3.11). This did not affect the pores in the lipid membrane. It has been already demonstrated before, that OT can be manipulated near a lipid membrane with -hemolysin by Lizarraga et al[85]. Although, no experiment combining -hemolysin and OT was demonstrated.
In our experiment, no DNA insertions were resolved in the bead dislocation trace (current trace could not be used, because there were many pores in the bilayer, and the total ion current was fluctuating). There might be several reasons, why the DNA did not translocate through the biopores.

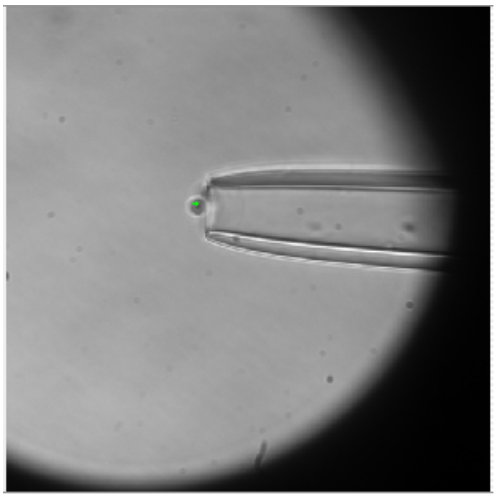

Figure 3.11: A bright field image of a captured optical bead near the capillary with multiple MspA pores in the bilayer. The green dot marks the approximate optical trap position.

The DNA construct was only verified by PCR amplification, but the yield is not known. Although, DNA length can be verified by the OT nanocapillary combination, ssDNA is immediately ejected from the capillary because of the electroosmotic flow. A special agarose-gel analysis has to be done, to resolve it. The length difference between the final construct and lambda DNA is insignificant to be noticed on a gel. A dye which binds single-stranded DNA would help to visualize the construct on the gel. Almost all single-stranded DNA dyes also bind double-stranded, which makes the gel analysis more

complicated, but there are dyes on the market, which have much higher preference for ssDNA (e.g. QuantiFluor ssDNA System). Another possibility is to use a fluorescent dye labelled linker. The linker would firstly be ligated to M13mp18 DNA, before ligating to Lambda. The product would be purified after each ligation. This way, we would be sure that we are using the correct construct, but each purification diminishes the yield.
Mention somwehere that we can not check in OT if the ssDNA part is there as it would be immediately ejected from the capillary due to the EOF, and that we can only check if the dsDNA is there.
The capture of the DNA also depends on the accessibility of the pore, meaning how far is the lipid membrane in the capillary. Lipid membranes cannot be visually distinguished. The capillary needs to be filled with a dye after bilayer formation. Food dyes cannot be seen in capillaries, because they are too thin to contain enough dye. However, fluorescent dyes, such as fluorescein, can be visualized at low quantities using a fluorescence microscope.
Having multiple pores in the bilayer increases the DNA capture probability. Normally, an optical bead is gradually moved along the capillary opening, till DNA is captured. With a large capillary, with a diameter in a few micrometre range, there is a much higher area to scan. Also, it is harder to capture the DNA in such a small pore compared to a nanocapillary whose diameters rarely go below 20 nm. Although, there should not be EOF flow effects on the DNA because of the lipid bilayer, and the size of the capillary (several micrometres).
In summary, we made progress towards the force measurement, but there are several aspects we have to investigate for the successful experiment. DNA construct must be analyzed, as well as lipid bilayer position in the capillary.

Conclusions 4

In this work, we devised an optical tweezers experiment to measure the force on DNA translocating through MspA. For this purpose a glass capillary was used to support the bilayer and the embedded biopore. We demonstrated that lipid membranes can be formed on our glass capillaries while working with PDMS chambers campatible with the optical tweezers setup. We have found that the bilayers stability is not affected by the laser beam nor the geometric peculiarities of the capillaries. We also were able to insert MspA pores in the bilayer and measure current-voltage characteristics, which were found to not be affected by the flow-cell peculiarities such as electroosmotic flow in capillaries. A construct was designed and produced which allowed combining ssDNA compatible with MspA, along with a base of dsDNA known to work with the OT setup. Unfortunately, we did not observe DNA capture using the optical tweezers and capillary combination.

The failure to controllably translocate the DNA with the OT might be caused by unsuccessful DNA construct synthesis or the membrane inaccessibility. The DNA construct might not have a long ssDNA part, or the long polymer could have been sheared during manipulations with a pipette. The construct has to be verified by gel electrophoresis with an ssDNA-specific dye. If this verification method does not work, the synthesis can be done step-wise with a fluorescently labelled linker, where each ligation is followed by a purification step. The translocations can also be limited by lipid membrane formation too far in the capillary, where the DNA on an optical bead length is insufficient to reach the biopores. The bilayer position can be detected by filling the trans chamber with a fluorescent dye and visualized with a fluorescence microscope. The position of the bilayer could then be controlled by applying hydrostatic pressure to the capillary, thus pushing the bilayer to a position close to the tip. For successful capture of the DNA, the distance between the bilayer and OT bead needs to be comparable to the size of the DNA. All these tests could be accomplished with additional time spent on the project.

Except for controlled translocations of DNA using the OT setup, we proved that each of the individual steps towards the force measurement work. Successful force measurement of DNA inside MspA would let us know the exact force values acting on DNA in SPRNT, which would considerably enhance the technique. In the future, we intend to calibrate the force on a DNA molecule translocating trough a nanopore for different temperature, salt concentration and driving voltages. The calibration would provide the force knowledge under different conditions, which would elucidate the motor protein kinetic behaviour.

Bibliography

1. Lohman, T. M. Helicase-catalyzed DNA unwinding. *Journal of Biological Chemistry* **268,** 2269–2272 (1993).
2. Kornberg, R. The molecular basis of eukaryotic transcription (Nobel Lecture). *Angewandte Chemie - International Edition* **46,** 6956–6965 (2007).
3. Becker, P. B. Nucleosome remodelers on track NEWS AND VIEWS. *Nature Structural & Molecular Biology* **12,** 732–733 (2005).
4. McClelland, S. E., Dryden, D. T. & Szczelkun, M. D. Continuous assays for DNA translocation using fluorescent triplex dissociation: Application to type I restriction endonucleases. *Journal of Molecular Biology* **348,** 895–915 (2005).
5. Kovall, R. A. & Matthews, B. W. Structural, functional, and evolutionary relationships between -exonuclease and the type II restriction endonucleases. *Proceedings of the National Academy of Sciences* **95,** 7893–7897 (2002).
6. McGhee, J. D. & von Hippel, P. H. Theoretical aspects of DNA-protein interactions: Co-operative and non-co-operative binding of large ligands to a one-dimensional homogeneous lattice. *Journal of Molecular Biology* **86,** 469–489 (1974).
7. Finkelstein, I. J. & Greene, E. C. Molecular Traffic Jams on DNA. *Annual Review of Biophysics* **42,** 241–263 (2013).
8. Huttner, D. & Hickson, I. D. Helicases. *Brenner's Encyclopedia of Genetics: Second Edition,* 406–408 (2013).
9. Tinoco, I. & Carlos, J. Reversible Unfolding of Single RNA Molecules by Mechanical Force Author (s): Jan Liphardt , Bibiana Onoa , Steven B . Smith , Ignacio Tinoco Jr . and Carlos Published by : American Association for the Advancement of Science Stable URL : http://www.jstor. **292,** 733–737 (2016).
10. Cecconi, C., Shank, E. A., Bustamante, C. & Marqusee, S. Supporting Online Material for Direct Observation of the Three-State Folding of a Single Protein Molecule. *Science* **2057** (2005).
11. Fourmond, V. *et al.* Dependence of catalytic activity on driving force in solution assays and protein film voltammetry: Insights from the comparison of nitrate reductase mutants. *Biochemistry* **49,** 2424–2432 (2010).
12. Alberts, B. & Alberts. *Molecular Biology of the Cell* English (2002).
13. Yang, H. *et al.* Protein Conformational Dynamics Probed by Single-Molecule Electron Transfer Sergio Cova , Luying Xun and X . Sunney Xie. **302,** 262–266 (2014).

14. Wang, Y. & Lu, H. P. Bunching effect in single-molecule T4 lysozyme nonequilibrium conformational dynamics under enzymatic reactions. *Journal of Physical Chemistry B* **114,** 6669–6674 (2010).

15. Bustamante, C., Smith, S. B., Liphardt, J. & Smith, D. Bustamante_CurrOpistructBiol_2002, 279–285 (2000).

16. Vale, R. D., Funatsu, T., Pierce, D. W. & Romberg, L. Direct observation of single kinesin molecules along microtubules. **380,** 451–453 (2010).

17. Van der Auweraer, M. *et al.* Stretched exponential decay and correlations in the catalytic activity of fluctuating single lipase molecules. *Proceedings of the National Academy of Sciences* **102,** 2368–2372 (2005).

18. Ha, T. *et al.* Ligand-induced conformational changes observed in single RNA molecules. *Proceedings of the National Academy of Sciences* **96,** 9077–9082 (2002).

19. Liem, L. K., Simard, J. M., Song, Y. & Tewari, K. The patch clamp technique. *Neurosurgery* **36,** 382–392 (1995).

20. Kier, N. & Nagy, A. Single-Molecule Force Spectroscopy: Optical Tweezers, Magnerit Tweezers and Atomic Force Microscopy. *National Institutes of Health* **5,** 491–505 (2012).

21. Ashkin, A., Dziedzic, J. M., Bjorkholm, J. E. & Chu, S. Kuvel et al. **11,** 288–290 (1986).

22. Zhang, H. & Liu, K. K. Optical tweezers for single cells. *Journal of the Royal Society Interface* **5,** 671–690 (2008).

23. Thacker, V. V. *et al.* Bacterial nucleoid structure probed by active drag and resistive pulse sensing. *Integrative Biology (United Kingdom)* **6,** 184–191 (2014).

24. Msz, K., Sb, S., Hl, G. & C, B. Folding-unfolding transitions in single titin molecules characterized with laser tweezers. *Science* **276,** 1112–46 (1997).

25. Heller, I., Hoekstra, T. P., King, G. A., Peterman, E. J. G. & Wuite, G. J. L. Optical Tweezers Analysis of DNA–Protein Complexes. *Chemical Reviews* **114,** 3087–3119 (2014).

26. Dholakia, K., Reece, P. & Gu, M. Optical micromanipulation. *Chemical Society Reviews* **37,** 42–55 (2008).

27. Reconditi, M. *et al.* The myosin motor in muscle generates a smaller and slower working stroke at higher load. *Nature* **428,** 578–581 (2004).

28. Roy, S., Dharmadhikari, J., Dharmadhikari, A., Mathur, D. & Sharma, S. Study of P. falciparum-infected erythrocytes and induced anisotropies under optical and fluid forces. *Journal of Vector Borne Diseases* **44,** 23–32 (2007).

29. Pralle, A., Prummer, M., Florin, E.-L., Stelzer, E. H. K. & Hörber, J. K. H. Three-dimensional position tracking for optical tweezers by forward scattered light. *Microscopy Research and Technique* **44,** 378–386 (1999).

30. Stein, B. P. All-optical trapping. *Physics Today* **55,** 9–9 (2007).

31. Capitanio, M. & Pavone, F. S. Interrogating biology with force: Single molecule high-resolution measurements with optical tweezers. *Biophysical Journal* **105,** 1293–1303 (2013).

32. Gebhardt, J. C. M., Bornschlogl, T. & Rief, M. Full distance-resolved folding energy landscape of one single protein molecule. *Proceedings of the National Academy of Sciences* **107,** 2013–2018 (2010).

33. Abbondanzieri, E. A., Greenleaf, W. J., Shaevitz, J. W., Landick, R. & Block, S. M. Direct observation of base-pair stepping by RNA polymerase. *Nature* **438,** 460–465 (2005).

34. Wanunu, M. Nanopores: A journey towards DNA sequencing. *Physics of Life Reviews* **9,** 125–158 (2012).

35. Feng, J. *et al.* Single-layer MoS2 nanopores as nanopower generators. *Nature* **536,** 197–200 (2016).

36. Heiranian, M., Farimani, A. B. & Aluru, N. R. Water desalination with a single-layer MoS 2 nanopore. *Nature Communications* **6,** 1–6 (2015).

37. Shui, W. *et al.* Nanopore-based proteolytic reactor for sensitive and comprehensive proteomic analyses. *Analytical Chemistry* **78,** 4811–4819 (2006).

38. Lotman, P. Identification and characterization of a cell membrane nucleic. **95,** 1921–1926 (1998).

39. Hall, J. E. Membrane Biology. *Science* **198,** 499–500 (2006).

40. Jung, M. K., Oakley, B. R. & Zheng, Y. Gamma-tubulin is present in Drosophila melanogaster and Homo sapiens and is associated with the centrosome. *Cell* **65,** 817–23 (1991).

41. Feng, Y., Zhang, Y., Ying, C., Wang, D. & Du, C. Nanopore-based fourth-generation DNA sequencing technology. *Genomics, Proteomics and Bioinformatics* **13,** 4–16 (2015).

42. Heng, J. B. *et al.* Sizing DNA using a nanometer-diameter pore. *Biophysical journal* **87,** 2905–2911 (2004).

43. Storm, A. J., Chen, J. H., Ling, X. S., Zandbergen, H. W. & Dekker, C. Fabrication of solid-state nanopores with single-nanometre precision. *Nature Materials* **2,** 537–540 (2003).

44. Venkatesan, B. M. & Bashir, R. Nanopore sensors for nucleic acid analysis. *Nature Nanotechnology* **6,** 615–624 (2011).

45. Liu, S. *et al.* Boron nitride nanopores: Highly sensitive DNA single-molecule detectors. *Advanced Materials* **25,** 4549–4554 (2013).

46. Garaj, S. *et al.* Graphene as a subnanometre trans-electrode membrane. *Nature* **467,** 190–193 (2010).

47. Menestrina, J., Yang, C., Schiel, M., Vlassiouk, I. & Siwy, Z. S. Charged particles modulate local ionic concentrations and cause formation of positive peaks in resistive-pulse-based detection. *Journal of Physical Chemistry C* **118,** 2391–2398 (2014).

48. Bai, J. *et al.* Fabrication of sub-20 nm nanopore arrays in membranes with embedded metal electrodes at wafer scales. *Nanoscale* **6,** 8900–8906 (2014).

49. Keyser, U. F. *et al.* Direct force measurements on DNA in a solid-state nanopore. *Nature Physics* **2,** 473–477 (2006).

50. Steinbock, L. J. *et al.* Probing DNA with micro- and nanocapillaries and optical tweezers. *Journal of Physics Condensed Matter* **22** (2010).

51. Otto, O., Steinbock, L. J., Wong, D. W., Gornall, J. L. & Keyser, U. F. Note: Direct force and ionic-current measurements on DNA in a nanocapillary. *Review of Scientific Instruments* **82,** 1–4 (2011).

52. Bulushev, R. D. *et al.* Single Molecule Localization and Discrimination of DNA-Protein Complexes by Controlled Translocation Through Nanocapillaries. *Nano Letters* **16,** 7882–7890 (2016).

53. Bulushev, R. D., Marion, S. & Radenovic, A. Relevance of the Drag Force during Controlled Translocation of a DNA-Protein Complex through a Glass Nanocapillary. *Nano Letters* **15,** 7118–7125 (2015).

54. Behrens, S. H. & Grier, D. G. The charge of glass and silica surfaces. *Journal of Chemical Physics* **115,** 6716–6721 (2001).

55. Laohakunakorn, N. & Keyser, U. F. Electroosmotic flow rectification in conical nanopores. *Nanotechnology* **26** (2015).

56. Steinbock, L. J. *et al.* Probing the size of proteins with glass nanopores. *Nanoscale* **6,** 14380–14387 (2014).

57. Mao, M., Sherwood, J. D. & Ghosal, S. Electro-osmotic flow through a nanopore. *Journal of Fluid Mechanics* **749,** 167–183 (2014).

58. Galla, L. *et al.* Hydrodynamic slip on DNA observed by optical tweezers-controlled translocation experiments with solid-state and lipid-coated nanopores. *Nano Letters* **14,** 4176–4182 (2014).

59. Sischka, A. *et al.* Controlled translocation of DNA through nanopores in carbon nano-, silicon-nitride- and lipid-coated membranes. *Analyst* **140,** 4843–4847 (2015).

60. Ermann, N. *et al.* Promoting single-file DNA translocations through nanopores using electro-osmotic flow. *Journal of Chemical Physics* **149** (2018).

61. Song, L., Hobaugh, M. R., Shustak, C., Cheley, S. & Gouaux, J. E. Structure of Staphylococcal α-Hemolysin , a Heptameric Transmembrane Pore Published by : American Association for the Advancement of Science Stable URL : http://www.jstor.org/stable/2891686. *Advancement Of Science* **274,** 1859–1866 (2008).

62. Wendell, D. *et al.* Translocation of double-stranded DNA through membrane-adapted phi29 motor protein nanopores. *Nature Nanotechnology* **4,** 765–772 (2009).

63. Butler, T. Z., Pavlenok, M., Derrington, I. M., Niederweis, M. & Gundlach, J. H. Single-molecule DNA detection with an engineered MspA protein nanopore. *Proceedings of the National Academy of Sciences* **105,** 20647–20652 (2008).

64. Laszlo, A. H., Derrington, I. M. & Gundlach, J. H. MspA nanopore as a single-molecule tool: From sequencing to SPRNT. *Methods* **105,** 75–89 (2016).

65. Derrington, I. M. *et al.* Subangstrom single-molecule measurements of motor proteins using a nanopore. *Nature Biotechnology* **33,** 1073–1075 (2015).

66. Heinz, C., Engelhardt, H. & Niederweis, M. The core of the tetrameric mycobacterial porin MspA is an extremely stable β-sheet domain. *Journal of Biological Chemistry* **278,** 8678–8685 (2003).

67. Manrao, E. A. *et al.* Reading DNA at single-nucleotide resolution with a mutant MspA nanopore and phi29 DNA polymerase. *Nature Biotechnology* **30,** 349–353 (2012).

68. Manrao, E. A., Derrington, I. M., Pavlenok, M., Niederweis, M. & Gundlach, J. H. Nucleotide discrimination with DNA immobilized in the MSPA nanopore. *PLoS ONE* **6,** 1–7 (2011).

69. Saeki, H. & Svejstrup, J. Q. Stability, Flexibility, and Dynamic Interactions of Colliding RNA Polymerase II Elongation Complexes. *Molecular Cell* **35,** 191–205 (2009).

70. Gravel, S. & Gunter, C. Interactions between RNA polymerase and the " core recognition. *Science* **344,** 1285–1290 (2014).

71. Craig, J. M. *et al.* Determining the effects of DNA sequence on Hel308 helicase translocation along single-stranded DNA using nanopore tweezers. *Nucleic acids research* **47,** 2506–2513 (2019).

72. Mueller, P., Rudin, D. O., Tien, H. T. & Wescott, W. C. Reconstitution of Excitable Cell Membrane Structure in Vitro. *Circulation* **26,** 1167–1171 (2012).

73. Siontorou, C. G., Nikoleli, G. P., Nikolelis, D. P. & Karapetis, S. K. Artificial lipid membranes: Past, present, and future. *Membranes* **7,** 1–24 (2017).

74. Montal, M. & Muellertj, P. Formation of Bimolecular Membranes from Lipid Monolayers and a Study of Their Electrical Properties (membrane structure/membrane reconstitution/asymmetric membranes/lipid bilayers). *Proceedings of the National Academy of Sciences of the United States of America* **69,** 3561–3566 (1972).

75. Hanke, W., Methfessel, C., Wilmsen, U. & Boheim, G. Ion channel reconstitution into lipid bilayer membranes on glass patch pipettes. *Bioelectrochemistry and Bioenergetics* **12,** 329–339 (1984).

76. Gutsmann, T., Heimburg, T., Keyser, U., Mahendran, K. R. & Winterhalter, M. Protein reconstitution into freestanding planar lipid membranes for electrophysiological characterization. *Nature Protocols* **10,** 188–198 (2015).

77. Gornall, J. L. *et al.* Simple reconstitution of protein pores in nano lipid bilayers. *Nano Letters* **11,** 3334–3340 (2011).

78. Marin, V., Kieffer, R., Padmos, R. & Aubin-Tam, M. E. Stable Free-Standing Lipid Bilayer Membranes in Norland Optical Adhesive 81 Microchannels. *Analytical Chemistry* **88,** 7466–7470 (2016).

79. Bulushev, R. Nanocapillaries combined with optical tweezers as a single molecule technique for studying DNA-protein complexes. **7608.** `https://infoscience.epfl.ch/record/227088/files/EPFL%7B%5C_%7DTH7608.pdf` (2017).

80. White, H. S., Schibel, A. E. P., Edwards, T., Kawano, R. & Lan, W. J. Quartz Nanopore Membranes for Suspended Bilayer Ion Channel Recordings. *Analytical Chemistry* **82,** 7259–7266 (2010).

81. Akeson, M., Branton, D., Kasianowicz, J. J., Brandin, E. & Deamer, D. W. Microsecond time-scale discrimination among polycytidylic acid, polyadenylic acid, and polyuridylic acid as homopolymers or as segments within single RNA molecules. *Biophysical Journal* **77,** 3227–3233 (1999).

82. Engelhardt, H., Heinz, C. & Niederweis, M. A tetrameric porin limits the cell wall permeability of Mycobacterium smegmatis. *Journal of Biological Chemistry* **277,** 37567–37572 (2002).

83. Huff, J., Pavlenok, M., Sukumaran, S. & Niederweis, M. Functions of the periplasmic loop of the porin MspA from Mycobacterium smegmatis. *Journal of Biological Chemistry* **284,** 10223–10231 (2009).

84. Bainbridge, G., Gokce, I. & Lakey, J. H. Voltage gating is a fundamental feature of porin and toxin β-barrel membrane channels. *FEBS Letters* **431,** 305–308 (1998).

85. Version, D. *Bridging the gap: combined optical tweezers with free standing lipid membrane* (2017).